

Supporting information for:

# Classifying and understanding the reactivities of Mo based alkyne metathesis catalysts from $^{95}\text{Mo}$ NMR chemical shift descriptors

*Zachariah J. Berkson,<sup>†</sup> Lukas Lätsch,<sup>†</sup> Julius Hillenbrand,<sup>‡</sup> Alois Fürstner,<sup>‡</sup> and Christophe Copéret<sup>\*†</sup>*

<sup>†</sup>*Department of Chemistry and Applied Biosciences, ETH Zürich, Zürich, Switzerland*

<sup>‡</sup>*Max-Planck-Institut für Kohlenforschung, 45470 Mülheim/Ruhr, Germany*

*E-mail: [ccoperet@ethz.ch](mailto:ccoperet@ethz.ch)*

## Table of Contents

S1. Experimental section .....	3
<i>S1.1. Synthetic protocols</i> .....	3
<i>S1.2. Solid-state NMR analyses</i> .....	6
<i>S1.3. DFT calculations</i> .....	7
S2. Solution NMR characterization of all complexes.....	8
<i>S2.1. Complex 1<sub>F0</sub></i> .....	8
<i>S2.2. Complex 1<sub>F3</sub></i> .....	11
<i>S2.3. Complex 1<sub>F6</sub></i> .....	17
<i>S2.4. Complex 1<sub>F9</sub></i> .....	23
<i>S2.5. Complex 2<sub>Ph</sub></i> .....	28
<i>S2.6. Complex 3<sub>Ph</sub></i> .....	33
<i>S2.7. Complex 3<sub>Et</sub></i> .....	37
<i>S2.8. Summary of Solution NMR data.</i> .....	41
S3. Solid-state <sup>95</sup> Mo NMR analyses .....	42
<i>S3.1. Experimental <sup>95</sup>Mo solid-state NMR spectra.</i> .....	42
<i>S3.2. Summary of <sup>95</sup>Mo solid-state NMR data.</i> .....	49
S4. DFT analyses.....	51
<i>S4.1. Summary of DFT calculations of <sup>95</sup>Mo NMR parameters.</i> .....	51
<i>S4.2. Benchmarking of DFT calculations.</i> .....	52
<i>S4.3. Orientations of chemical shielding tensors.</i> .....	53
<i>S4.4. Natural Chemical Shift analysis.</i> .....	55
<i>S4.5. Calculated HOMO and LUMO energies of all complexes</i> .....	60
<i>S4.6. Natural charge analysis.</i> .....	61
<i>S4.7. Influence of geometry and ligand substituents on <sup>95</sup>Mo NMR parameters.</i> .....	61
References .....	65

## S1. Experimental section

### S1.1. Synthetic protocols

**General.** Unless stated otherwise, all reactions were carried out under Ar in flame-dried glassware. The solvents were purified by distillation over the drying agents indicated and were transferred under Ar: THF, Et<sub>2</sub>O (Mg/anthracene), CH<sub>2</sub>Cl<sub>2</sub>, DME (CaH<sub>2</sub>), *n*-pentane, benzene, toluene (Na/K).

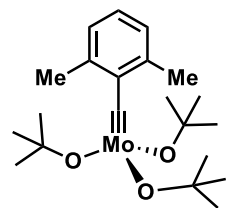
All commercially available compounds (Fluka, Lancaster, Aldrich) were used as received, unless stated otherwise.

IR: Spectrum One (Perkin-Elmer) spectrometer, wavenumbers ( $\tilde{\nu}$ ) in cm<sup>-1</sup>. MS (EI): Finnigan MAT 8200 (70 eV), ESI-MS: ESQ3000 (Bruker), accurate mass determinations: Bruker APEX III FT-MS (7 T magnet) or Mat 95 (Finnigan). Elemental analysis: H. Kolbe, Mülheim/Ruhr.

Solution-phase NMR: Spectra were acquired on Bruker AvanceIII 300, 400, 500 MHz or AVneo 600 MHz NMR spectrometers in the solvents indicated; the AVneo 600 MHz NMR spectrometer was equipped with a Bruker BBO CryoProbe. Chemical shifts ( $\delta$ ) are given in ppm relative to TMS, coupling constants ( $J$ ) in Hz. The solvent signals were used as references and the chemical shifts converted to the TMS scale (CD<sub>2</sub>Cl<sub>2</sub>:  $\delta_C \equiv 53.8$  ppm; residual CHDCl<sub>2</sub>:  $\delta_H \equiv 5.32$  ppm; C<sub>6</sub>D<sub>6</sub>:  $\delta_C \equiv 128.1$  ppm; residual C<sub>6</sub>HD<sub>5</sub>:  $\delta_H \equiv 7.16$  ppm; [D<sub>8</sub>]-toluene:  $\delta_C \equiv 20.4$  ppm; residual D<sub>5</sub>C<sub>6</sub>CD<sub>2</sub>H:  $\delta_H \equiv 2.09$  ppm). <sup>19</sup>F NMR shifts were referenced indirectly to the <sup>1</sup>H NMR frequency of the sample with the 'xiref'-macro in Bruker TOPSPIN; they are given relative to  $\delta(\text{CFCl}_3) \equiv 0$  ppm ( $\Xi(^{19}\text{F}) = 94.094011\%$ ).

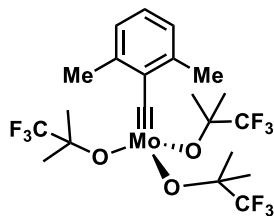
Solution-phase <sup>95</sup>Mo NMR spectra were acquired with the aring pulse sequence to minimize acoustic ringing from the NMR probe. The  $\pi/2$  pulse was calibrated for a 2 M Na<sub>2</sub>MoO<sub>4</sub> in D<sub>2</sub>O and had a typical length of 22.5  $\mu\text{s}$  at a power of 85 W. Chemical shifts were referenced indirectly to the <sup>1</sup>H chemical shift of the solvent.<sup>1</sup> Dependent on the line width of the signal, 8000 to 150000 FID containing 8192 complex data points were averaged to obtain a reasonable signal-to-noise ratio. The acquisition time of a single FID was around 150 ms. The data was Fourier-transformed with zero-filling to 8192 data points and with a line broadening lb = 20 Hz, unless noted otherwise.

### Preparation of the Complexes.

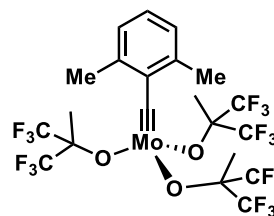


**Complex 1Fo.**<sup>2</sup> A 250 mL Schlenk flask equipped with a magnetic stir bar was flame dried under vacuum. The flask was filled with argon and charged with Mo( $\equiv$ CAr)Br<sub>3</sub>(dme) (Ar = 2,6-dimethylphenyl)<sup>3</sup> (2.05 g, 3.79 mmol) and THF (23 mL). A solution of NaOtBu (1.07 g, 11.2 mmol) in THF (7 mL) was added dropwise at ambient temperature and the resulting mixture was stirred for 14 h before the solvent was removed in vacuum to obtain a dark brown solid. This residue was suspended in *n*-pentane (4 x 20 mL) and the suspension was filtered under Ar through a pad of Celite<sup>®</sup> into a flame-dried 250 mL two-necked flask connected to an Ar-manifold. The filter frit was replaced by a stopper and the filtrate was concentrated in vacuum to a total volume of ca. 4 mL. The flask containing this concentrated solution was immersed into a cooling bath set to -40°C, leading to the precipitation of the title complex over the course of ca. 4 h. The supernatant was carefully removed via cannula and the residue dried in high vacuum to give the title complex as a brown solid material (1.31 g, 80%). <sup>1</sup>H NMR (400 MHz, C<sub>6</sub>D<sub>6</sub>):  $\delta = 6.90$  (dd,  $J = 7.3, 0.8$  Hz, 2H), 6.80 (dd,  $J = 8.2, 6.8$  Hz, 2H), 2.86 (s, 6H), 1.44 (s, 27H). <sup>13</sup>C NMR (101 MHz, C<sub>6</sub>D<sub>6</sub>):  $\delta = 297.1, 145.5, 139.4, 127.4, 127.1, 78.7, 32.3, 21.0$ . <sup>95</sup>Mo NMR (26 MHz, [D<sub>8</sub>]-toluene,

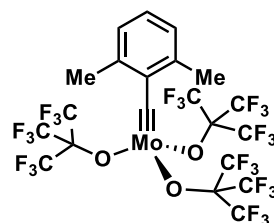
333 K):  $\delta = 259.0$ . IR (film):  $\tilde{\nu}$  2969, 2923, 1461, 1359, 1383, 1236, 1162, 1099, 1025, 946, 895, 765, 788, 732, 640, 575, 591, 475, 412  $\text{cm}^{-1}$ . The recorded data match the literature.<sup>2</sup>



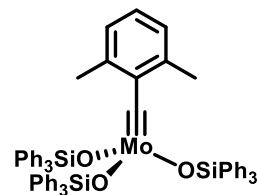
**Complex 1F3.** A suspension of sodium trifluoro-*tert*-butoxide (172.8 mg, 1.15 mmol) in toluene (4 mL) was added to a solution of  $\text{Mo}(\equiv\text{CAr})\text{Br}_3(\text{dme})$  ( $\text{Ar} = 2,6\text{-dimethylphenyl}$ )<sup>3</sup> (205 mg, 0.378 mmol) in toluene (8 mL) and the resulting mixture was stirred at ambient temperature overnight. The solvent was evaporated and the crude pale brown material was extracted with pentane. The combined pentane fractions were evaporated and the residue was dried in vacuum to give the title complex as a colorless solid (170 mg, 76%); because of the high solubility in organic solvents, traces of trifluoro-*tert*-butanol and 1,2-bis(2,6-dimethylphenyl)ethyne (formed by dimerization of the alkylidyne unit)<sup>2</sup> could not be fully removed by re-crystallization or extraction. <sup>1</sup>H NMR (600 MHz, [D<sub>8</sub>]-toluene):  $\delta = 6.72 - 6.74$  (m, 3H), 2.62 (s, 6H), 1.42 (s, 18H). <sup>13</sup>C NMR (151 MHz, [D<sub>8</sub>]-toluene):  $\delta = 306.7, 145.0, 140.2, 128.9, 127.6, 126.8$  ( $J = 284.8$  Hz), 81.3 ( $J = 28.9$  Hz), 24.4, 20.8. <sup>19</sup>F NMR (282 MHz, [D<sub>8</sub>]-toluene):  $\delta = -82.8$ . <sup>95</sup>Mo NMR (26 MHz, [D<sub>8</sub>]-toluene, 333 K):  $\delta = 319.7$ . MS (ESI+): 291 (21), 275 (18), 263 (95), 259 (100), 247 (15), 243 (12), 151 (48).



**Complex 1F6.** Prepared analogously as a white solid material (342 mg, quant.). <sup>1</sup>H NMR (600 MHz, [D<sub>8</sub>]-toluene):  $\delta = 6.64 - 6.71$  (m, 3H), 2.50 (s, 6H), 1.54 (s, 9H). <sup>13</sup>C NMR (151 MHz, [D<sub>8</sub>]-toluene):  $\delta = 317.2, 145.0, 141.7, 130.6, 127.8, 123.5$  ( $J = 287.5$  Hz), 83.9 ( $J = 30.1$  Hz), 20.4, 18.3. <sup>19</sup>F NMR (282 MHz, [D<sub>8</sub>]-toluene):  $\delta = -78.2$ . <sup>95</sup>Mo NMR (26 MHz, [D<sub>8</sub>]-toluene, 333 K):  $\delta = 432.7$ . MS (APPIpos.): 234 (100), 149 (8), 135 (7), 133 (7), 120 (12). Elemental analysis (%) calculated for  $\text{C}_{21}\text{H}_{18}\text{F}_{18}\text{MoO}_3$ : C 33.35, H 2.40, F 45.22, Mo 12.69; found: C 33.03, H 2.43, F 44.87, Mo 12.59.

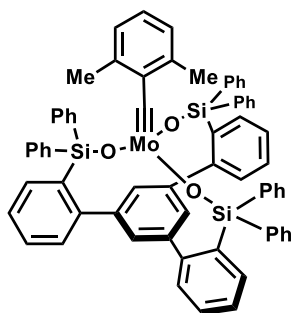


**Complex 1F9.** Prepared analogously as a white solid material (291 mg, 98%). <sup>1</sup>H NMR (400 MHz, [D<sub>8</sub>]-toluene):  $\delta = 6.56 - 6.60$  (m, 1H), 6.50 - 6.57 (m, 2H), 2.49 (s, 6H). <sup>13</sup>C NMR (151 MHz, [D<sub>8</sub>]-toluene):  $\delta = 332.9, 145.2, 143.5, 132.1$  ( $J = 160.6$  Hz), 127.6, 121.0 ( $J = 291.0$  Hz), 85.8 ( $J = 31.0$  Hz), 19.8. <sup>19</sup>F NMR (565 MHz, [D<sub>8</sub>]-toluene):  $\delta = -73.7$ . <sup>95</sup>Mo NMR (26 MHz, [D<sub>8</sub>]-toluene, 333 K):  $\delta = 691.1$ . MS (EI): 920 (4), 919 (2), 918 (3), 917 (3), 704 (6), 703 (4), 703 (5), 701 (5), 700 (3), 277 (11), 238 (10), 236 (14), 235 (25), 234 (91), 233 (17), 228 (25), 220 (11), 219 (55), 218 (23), 215 (11), 205 (10), 204 (55), 203 (30), 202 (29), 197 (21), 181 (14), 167 (13), 147 (24), 133 (31), 117 (81), 115 (77), 105 (25), 97 (32), 69 (100). HRMS-ESI ( $m/z$ ): calculated for  $\text{C}_{24}\text{H}_{18}\text{F}_{26}\text{MoO}_3^+$ , 919.91773; found 919.91577.



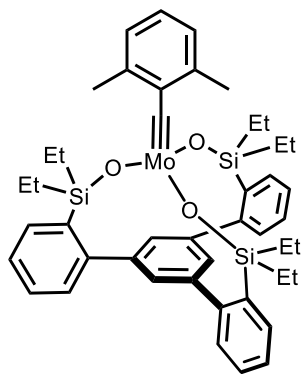
**[(Ph<sub>3</sub>SiO)<sub>3</sub>Mo(≡CAr)] (Ar = 2,6-Dimethylphenyl) (2Ph).**<sup>3</sup> A solution of Ph<sub>3</sub>SiOK (846 mg, 2.69 mmol) in THF (54 mL) was added via a dropping funnel over the course of 4 h to a solution of  $\text{Mo}(\equiv\text{CAr})\text{Br}_3(\text{dme})$  ( $\text{Ar} = 2,6\text{-dimethylphenyl}$ )<sup>3</sup> (490 mg, 0.903 mmol) in THF (46 mL) at 0°C. Once the addition was complete, the cooling bath was removed and stirring was continued for 1 h before the solvent was evaporated. The residue was suspended in toluene (30 mL) and the resulting slurry filtered through a pad of Celite<sup>®</sup>, which was carefully rinsed with additional toluene (15 mL). The combined filtrates were evaporated and the residue was dried in high vacuum. The crude product was dissolved in

Et<sub>2</sub>O (40 mL) and the resulting solution gently stirred at 0°C, which resulted in the formation of a yellow precipitate, which was filtered off under Ar, washed with cold Et<sub>2</sub>O (20 mL), and dried in vacuum to give the title complex as a yellow solid material (578 mg, 62%). <sup>1</sup>H NMR (600 MHz, [D<sub>8</sub>]-toluene): δ = 7.67 (m, 18H), 7.13 (m, 9H), 7.05 (m, 18H), 6.50 (t, *J* = 7.6 Hz, 1H), 6.43 (m, 2H), 1.87 (s, 6H). <sup>1</sup>H NMR (400 MHz, CD<sub>2</sub>Cl<sub>2</sub>): δ = 7.56 (d, *J* = 7.2 Hz, 18H), 7.36 (t, *J* = 7.8 Hz, 9H), 7.21 (t, *J* = 7.4 Hz, 18H), 6.64 (t, *J* = 7.6 Hz, 1H), 6.55 (dd, *J* = 7.6, 0.6 Hz, 2H), 1.71 (s, 6H). <sup>13</sup>C NMR (151 MHz, [D<sub>8</sub>]-toluene): δ = 306.9, 144.4, 139.1, 135.7, 135.2, 129.7, 127.6, 127.1, 125.8, 19.9. <sup>13</sup>C NMR (100 MHz, CD<sub>2</sub>Cl<sub>2</sub>): δ = 307.3, 144.7, 139.6, 136.7, 136.5, 136.0, 135.8, 135.5, 135.4, 135.2, 130.5, 130.3, 129.8, 128.7, 128.3, 128.1, 127.7, 127.2, 126.1, 20.2. <sup>29</sup>Si NMR (79 MHz, C<sub>6</sub>D<sub>5</sub>CD<sub>3</sub>): δ = -8.7. <sup>95</sup>Mo NMR (26 MHz, [D<sub>8</sub>]-toluene, 333 K): δ = 475.6. The recorded data match the literature.<sup>3</sup>



**Complex 3<sub>Ph</sub>.**<sup>2</sup> A 100 mL Schlenk flask equipped with a magnetic stir bar and connected to an Ar/vacuum manifold was flame dried under vacuum. The flask was filled with argon and charged with the tripodal silanol (388 mg, 0.431 mmol),<sup>2</sup> which was azeotropically dried with benzene (3 x 5 mL) to remove residual water. Toluene (32 mL) was added and the mixture was vigorously stirred for 10 min to obtain a clear solution. A solution of complex F0 (192 mg, 0.444 mmol) in toluene (6 mL) was added dropwise and stirring was continued for 6 h at ambient temperature. The solvent was removed under vacuum and the resulting yellow/orange solid material was washed with *n*-pentane (3 x 5 mL)

and Et<sub>2</sub>O (3 x 5 mL) to give the title complex as a yellow/orange powder (312 mg, 65%). <sup>1</sup>H NMR (400 MHz, [D<sub>8</sub>]-toluene): δ = 7.81 – 7.76 (m, 12H), 7.76 – 7.72 (m, 3H), 7.23 (s, 3H), 7.13 – 7.00 (m, 24H), 6.87 – 6.81 (m, 3H), 6.37 (s, 3H), 1.95 (s, 6H). <sup>13</sup>C NMR (101 MHz, [D<sub>8</sub>]-toluene): δ = 312.2, 149.2, 144.8, 143.8, 138.6, 137.5, 137.1, 134.8, 134.6, 130.1, 129.7, 129.4, 128.7, 127.6, 127.2, 125.8, 125.6, 19.7. <sup>29</sup>Si NMR (79 MHz, C<sub>6</sub>D<sub>5</sub>CD<sub>3</sub>): δ = -9.4. <sup>95</sup>Mo NMR (26 MHz, 333 K, [D<sub>8</sub>]-toluene): δ = 466.8. IR (film):  $\tilde{\nu}$  1428, 1112, 1086, 1020, 1032, 997, 875, 849, 736, 772, 443, 413 cm<sup>-1</sup>. HRMS-ESI (*m/z*): calculated for C<sub>69</sub>H<sub>55</sub>MoO<sub>3</sub>Si<sub>3</sub><sup>+</sup> [M+H]<sup>+</sup>, 1113.25076; found, 1113.25104. Elemental analysis (%) calculated for C<sub>69</sub>H<sub>54</sub>MoO<sub>3</sub>Si<sub>3</sub>: C 74.57, H 4.90, Mo 8.63; found: C 74.45, H 5.06, Mo 9.13. The recorded data match the literature.<sup>2</sup>



**Complex 3<sub>Et</sub>.**<sup>4</sup> Prepared analogously as a yellow/orange powder (1.63 g, 99%, ca. 97% pure according to NMR). <sup>1</sup>H NMR (600 MHz, [D<sub>8</sub>]-toluene): δ = 7.44 (s, 3H), 7.43 – 7.39 (m, 3H), 7.26 – 7.21 (m, 3H), 7.20 – 7.14 (m, 6H), 6.80 – 6.76 (m, 2H), 6.65 (t, *J* = 7.5 Hz, 1H), 2.68 (s, 6H), 1.01 – 0.96 (m, 18H), 0.95 – 0.86 (m, 12H). <sup>13</sup>C NMR (151 MHz, [D<sub>8</sub>]-toluene): δ = 305.8, 149.2, 145.0, 144.2, 137.9, 135.9, 134.2, 130.4, 128.6, 127.6, 127.0, 126.3, 126.2, 20.4, 9.1, 6.8. <sup>29</sup>Si NMR (119 MHz, [D<sub>8</sub>]-toluene): δ = 11.8. <sup>95</sup>Mo NMR (26 MHz, 60°C, [D<sub>8</sub>]-toluene): δ = 416.9. IR (film):  $\tilde{\nu}$  3051, 2952, 2931, 2909, 2872, 1581, 1557, 1460, 1429, 1407, 1375, 1259, 1232, 1161, 1122, 1088, 1063, 1044, 1012, 1002, 912, 761, 725, 697, 668, 624, 584, 552, 528, 513, 479, 460, 420 cm<sup>-1</sup>. HRMS-

ESI (*m/z*): calculated for C<sub>45</sub>H<sub>54</sub>MoO<sub>3</sub>Si<sub>3</sub><sup>+</sup> [M]<sup>+</sup>: 824.24293; found, 824.24333. The recorded data match the literature.<sup>4</sup>

### *S1.2. Solid-state NMR analyses*

The solid-state  $^{95}\text{Mo}$  NMR spectra were all acquired on a Bruker Avance III 600 MHz (14.1 T) DNP NMR spectrometer equipped with a low-temperature 3.2 mm triple-resonance MAS cryoprobe operating at Larmor frequencies of 599.900 and 39.0559 MHz for  $^1\text{H}$  and  $^{95}\text{Mo}$ , respectively. In an Ar-filled glovebox, each compound was packed into a sapphire MAS NMR rotor with a zirconia cap, transferred to the NMR spectrometer in a tightly sealed vial with a screw-cap top and rapidly inserted into the pre-cooled (100 K) MAS NMR probe head. Spectra at different MAS rates were measured to allow for determination of the chemical shift tensor components as well as estimation of the Euler angles and efg tensors. Spectra were acquired under MAS (5 kHz to 10 kHz) using a rotor synchronized  $\pi/2$ - $\tau$ - $\pi$ - $\tau$  echo sequence with  $\tau = 1$  or 2 rotor periods and with a double frequency sweep<sup>5</sup> in the preparatory period and QCPMG detection<sup>6</sup> to enhance sensitivity. Typically, 25 kHz central transition (CT)-selective pulses were used, with 10-20 echoes detected in the QCPMG train and a number of transients selected based on the observed sensitivity. Table S1.1 lists the number of transients acquired for each spectrum. For complexes **1F9**, **3Ph**, and **3Et**, the very large CSA precluded excitation of the full lineshape using CT selective pulses and severely limited sensitivity. For these compounds, static spectra were also acquired using a broadband WURST-QCPMG sequence<sup>7</sup> with 50  $\mu\text{s}$  200 kHz WURST pulses. WURST-QCPMG spectra were acquired with high-to-low and low-to-high frequency sweeps, which were co-added. Even using wideband excitation methods, sensitivity for complex **3Ph** was severely limited despite very long acquisition times, likely due to the broad lineshape and relatively low Mo content of this complex. Table S3.1 includes approximate uncertainties on experimentally measured parameters. All spectra were phased by magnitude correction. Lineshape simulations were performed using DMFIT software.<sup>8</sup>

Table S1.1. Number of transients acquired for each solid-state  $^{95}\text{Mo}$  NMR spectrum. All spectra were acquired at 14.1 T and 100 K with a 10 s relaxation delay and using a DFS-enhanced QCPMG-echo sequence under MAS or a broadband WURST-QCPMG pulse sequence for static measurements.

Compound	MAS rate (kHz)	No. transients
<b>1<sub>F0</sub></b>	10	1800
<b>1<sub>F0</sub></b>	5	5392
<b>1<sub>F3</sub></b>	10	6000
<b>1<sub>F3</sub></b>	8	2128
<b>1<sub>F3</sub></b>	5	6848
<b>1<sub>F6</sub></b>	10	4548
<b>1<sub>F6</sub></b>	5	7788
<b>1<sub>F9</sub></b>	10	13952
<b>1<sub>F9</sub></b>	0 (static)	15680
<b>2<sub>Ph</sub></b>	10	4940
<b>2<sub>Ph</sub></b>	8	22400
<b>2<sub>Ph</sub></b>	5	7760
<b>3<sub>Ph</sub></b>	10	8768
<b>3<sub>Ph</sub></b>	0 (static)	51136
<b>3<sub>Et</sub></b>	10	8500
<b>3<sub>Et</sub></b>	5	16468
<b>3<sub>Et</sub></b>	0 (static)	34048

### *S1.3. DFT calculations*

Geometry optimization and natural population analysis calculations were performed with the B3LYP<sup>9</sup> functional in combination with the 6-31g(d)<sup>10</sup> and lanl2dz<sup>11</sup> basis sets for main group elements and Mo, respectively using the Gaussian09 (revision d1) program suite.<sup>12</sup> Crystal structures were used as starting points for the calculations for complexes **2<sub>Ph</sub>** (CCDC no. 846113), **3<sub>Et</sub>** (CCDC no. 2088379), and **3<sub>Ph</sub>** (CCDC no. 1987913); for the fluoroalkoxide complexes the W analogue of **1<sub>F0</sub>** was used as a starting point (CCDC no. 2013167). Chemical shift calculations were performed with the ADF 2014<sup>17</sup> code using the revised Perdew-Burke-Entzerhof<sup>13</sup> in combination with a DZP basis set and TZ2P<sup>18</sup> basis set - for main group elements and Mo, respectively - with the all-electron relativistic zeroth-order regular approximation (ZORA)<sup>19</sup> in its spin-orbit two-component form. For the natural localized molecular orbitals (NLMO) analysis of the principal components of the chemical shielding tensor, the NBO 6.0<sup>20</sup> code is used as implemented in ADF 2014 with the revised Perdew-Burke-Entzerhof<sup>13</sup> functional and TZ2P<sup>18</sup>

basis set. The chemical shift of  $^{95}\text{Mo}$  derived from the computed  $^{95}\text{Mo}$  chemical shielding was obtained via linear regression of experimental and computed values (see section S4.2).

## S2. Solution NMR characterization of all complexes

### S2.1. Complex **1F0**

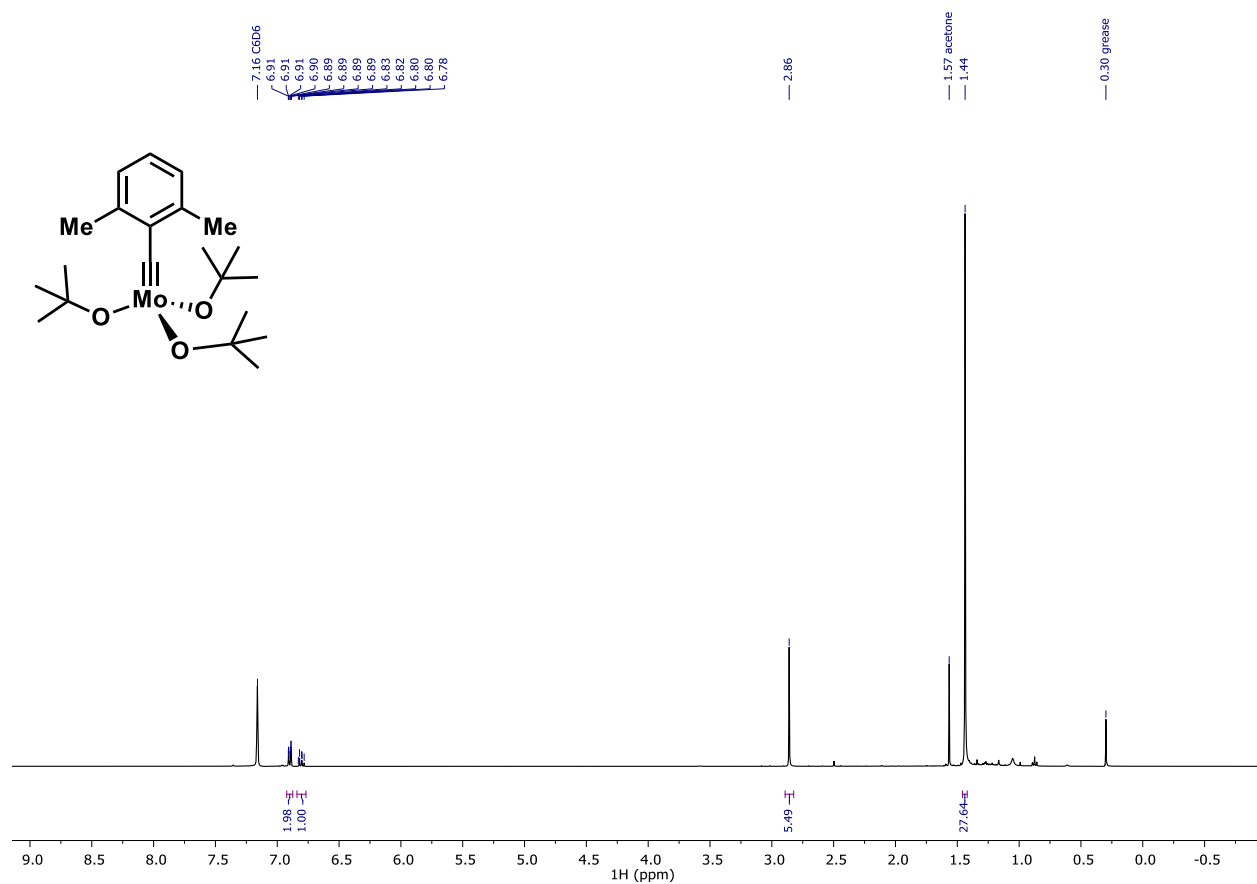


Figure S1.  $^1\text{H}$  NMR spectrum of Complex **1F0**, 400 MHz,  $\text{C}_6\text{D}_6$ ,  $25^\circ\text{C}$ .



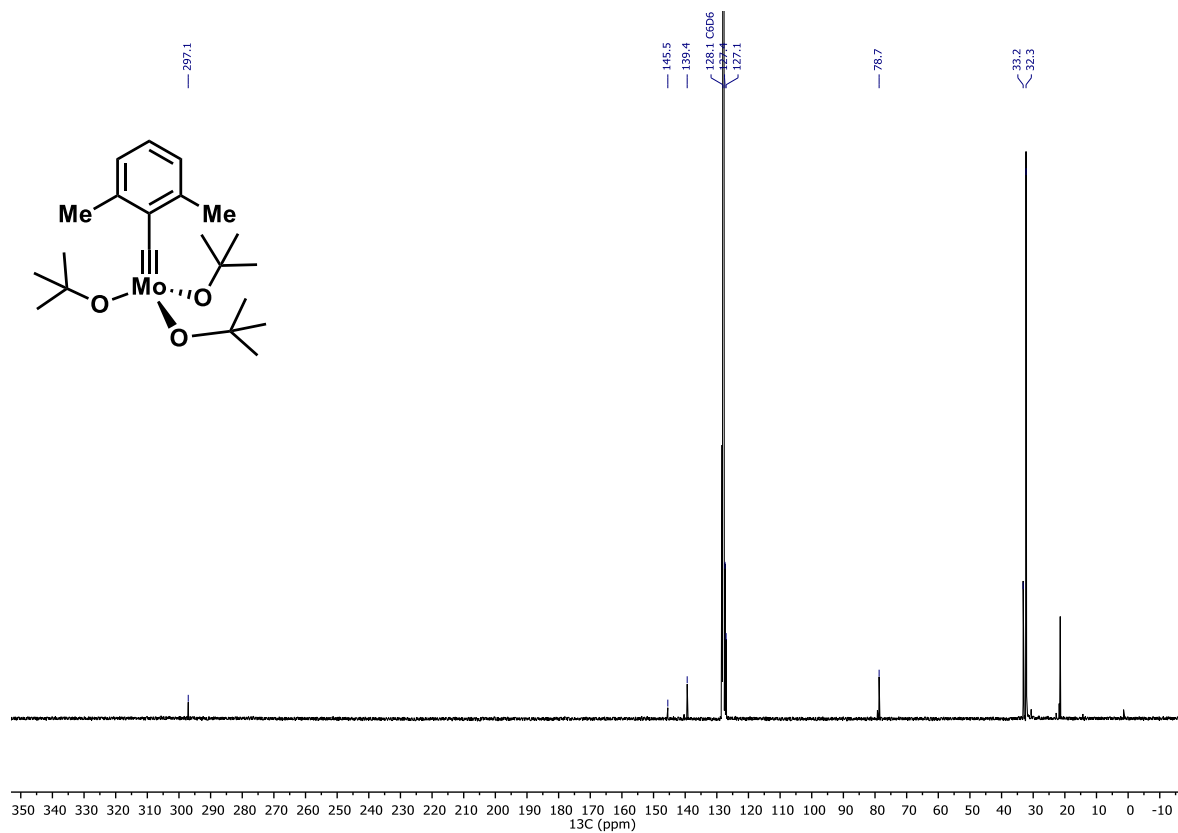


Figure S2.  $^{13}\text{C}$  NMR spectrum of Complex **1F0**, 101 MHz,  $\text{C}_6\text{D}_6$ , 25°C.

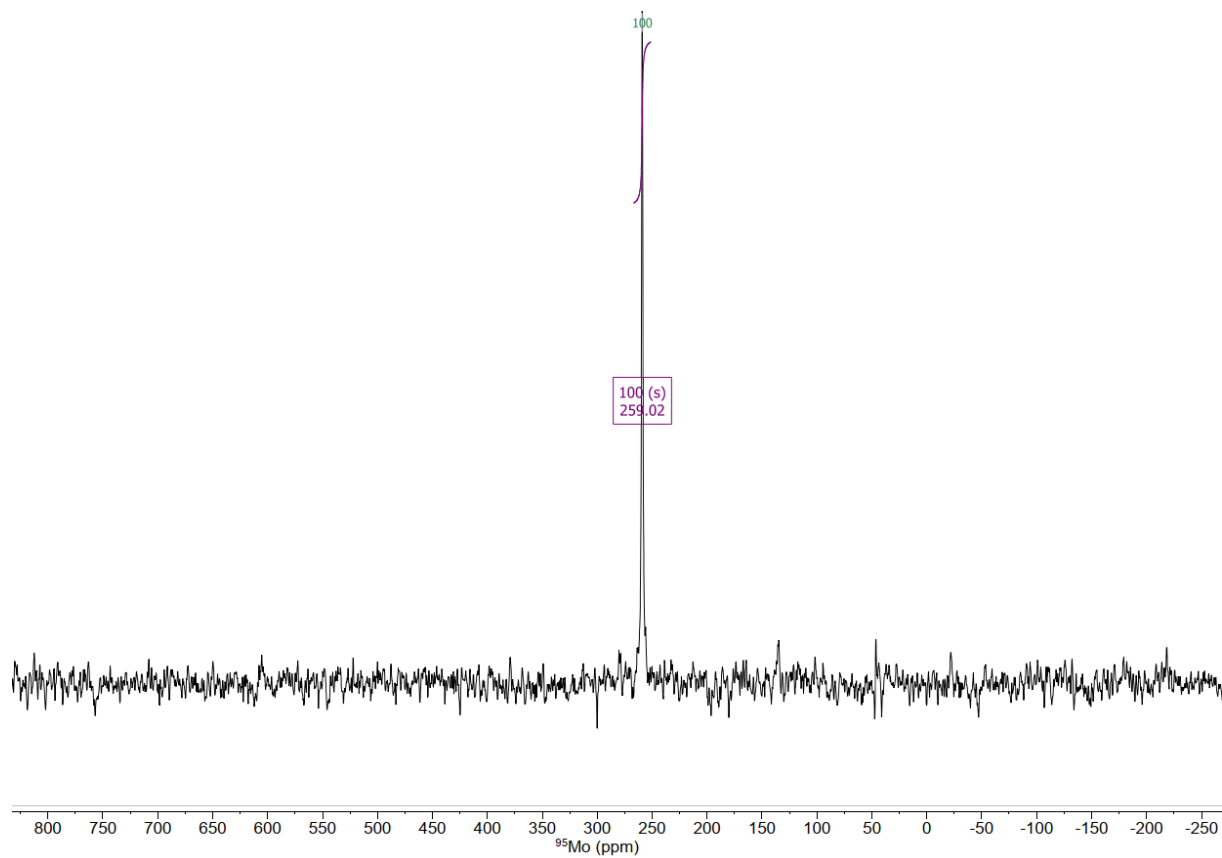


Figure S3.  $^{95}\text{Mo}$  NMR spectrum of Complex **1F0**, 26 MHz,  $[\text{D}_8]$ -toluene, 60°C.

## S2.2. Complex **1F3**

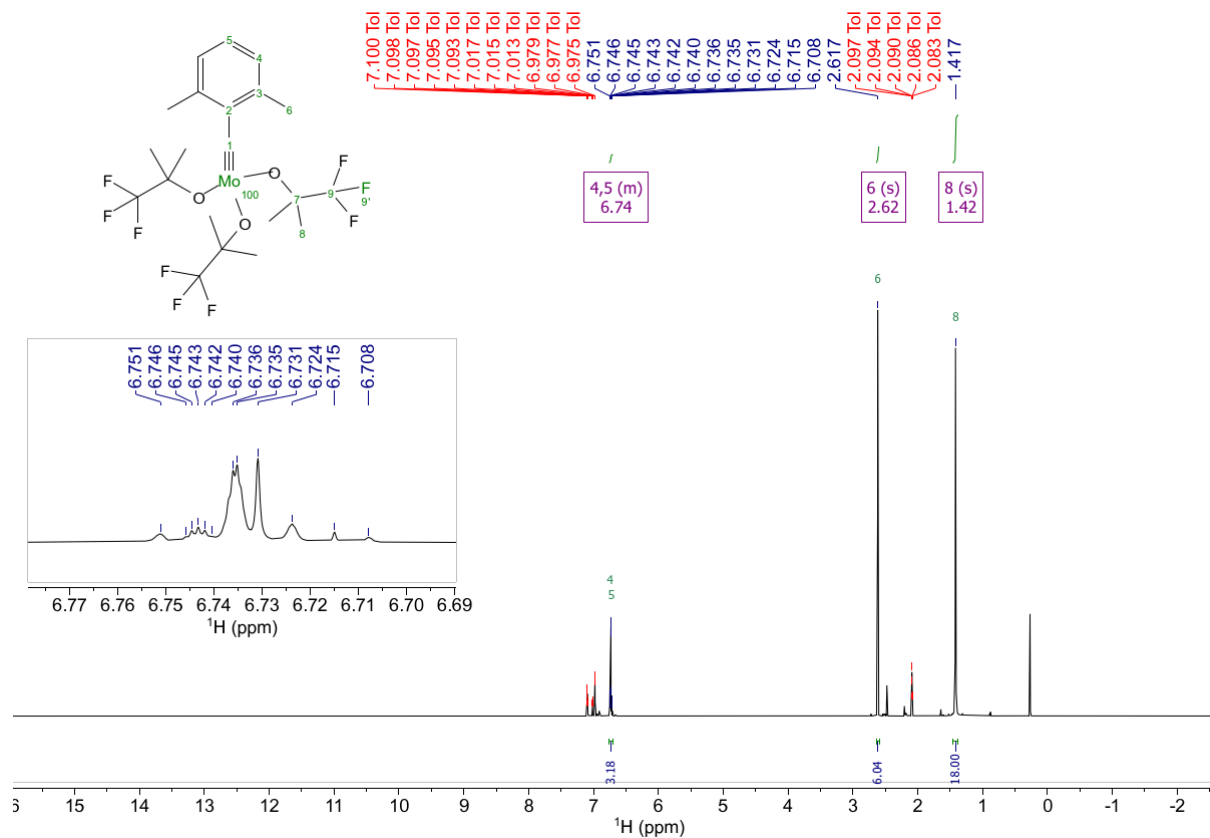


Figure S4.  $^1\text{H}$  NMR spectrum of Complex **1F3**, 600 MHz,  $[\text{D}_8]$ -toluene, 25°C,  $\approx 95\%$  pure (see text) (arbitrary numbering as shown).

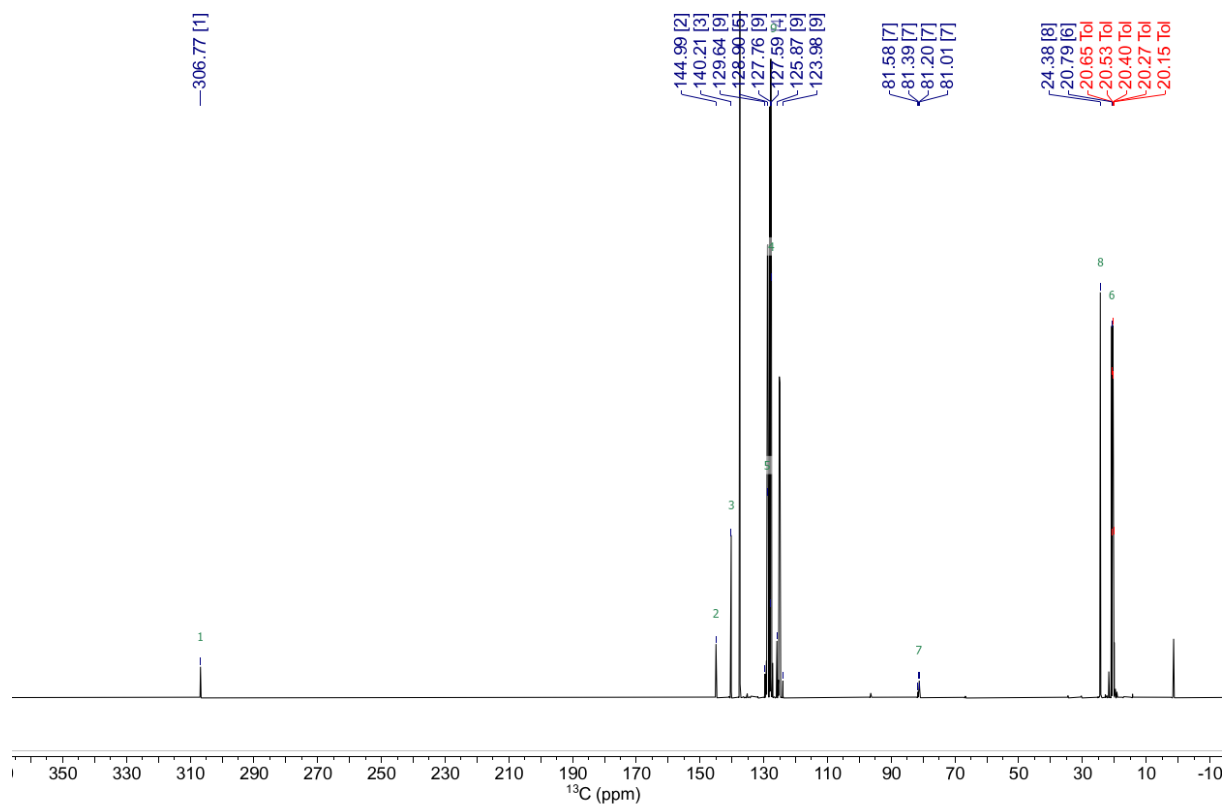


Figure S5.  $^{13}\text{C}$  NMR spectrum of Complex **1F3**, 151 MHz,  $[\text{D}_8]$ -toluene, 25°C,  $\approx 95\%$  pure (see text) (*arbitrary numbering*).

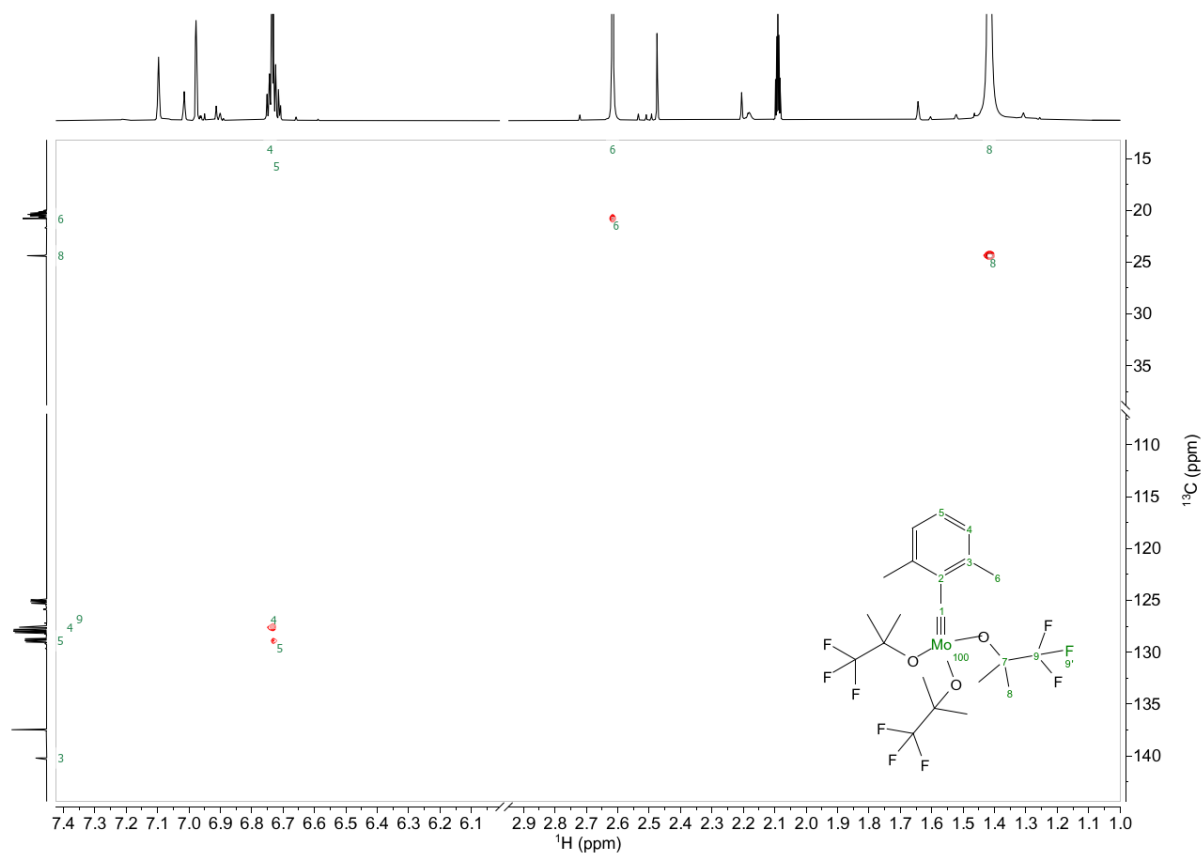


Figure S6.  $^1\text{H}$ - $^{13}\text{C}$ -HMQC spectrum of Complex  $1_{\text{F}3}$ , 600 MHz,  $[\text{D}_8]$ -toluene, 25°C,  $\approx 95\%$  pure (see text) (*arbitrary numbering*).

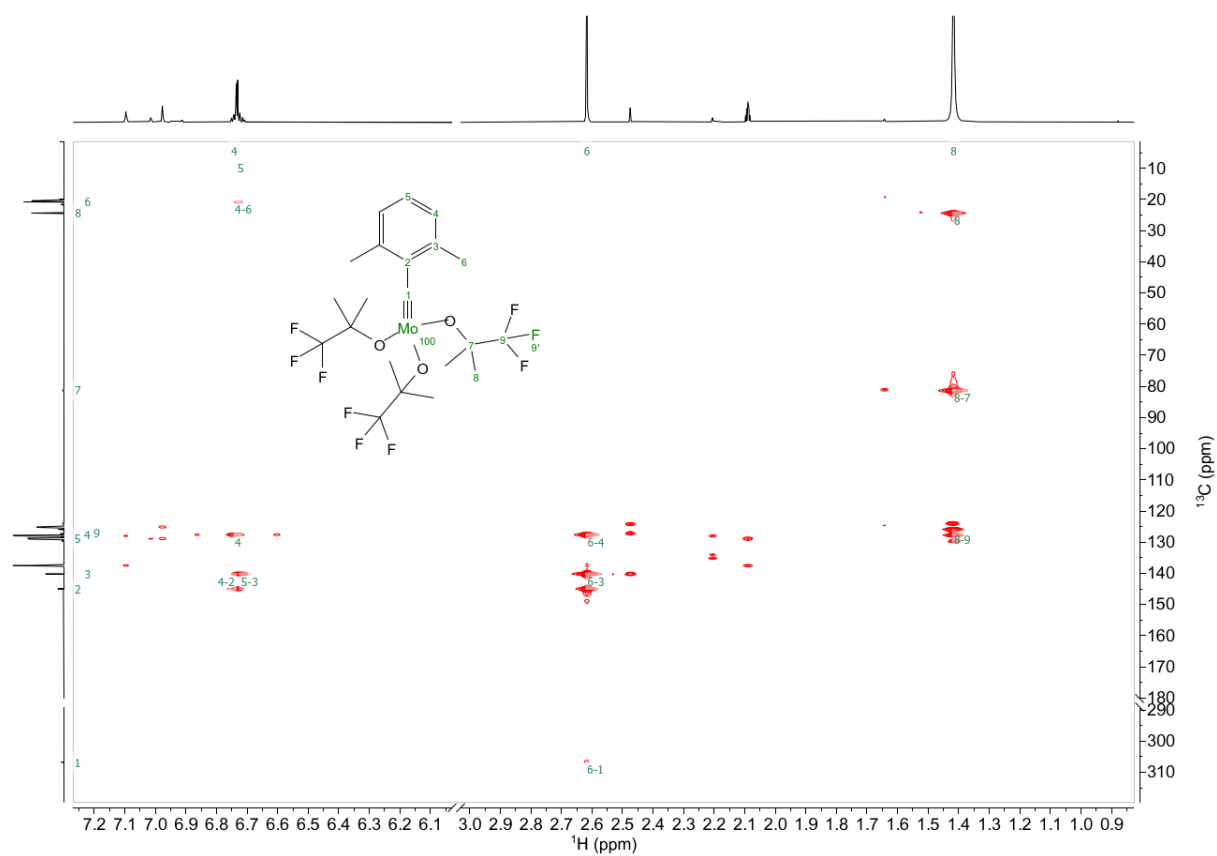


Figure S7.  $^1\text{H}$ - $^{13}\text{C}$ -HMBC spectrum of Complex **1F3**, 600 MHz,  $[\text{D}_8]$ -toluene, 25°C,  $\approx 95\%$  pure (see text) (arbitrary numbering).

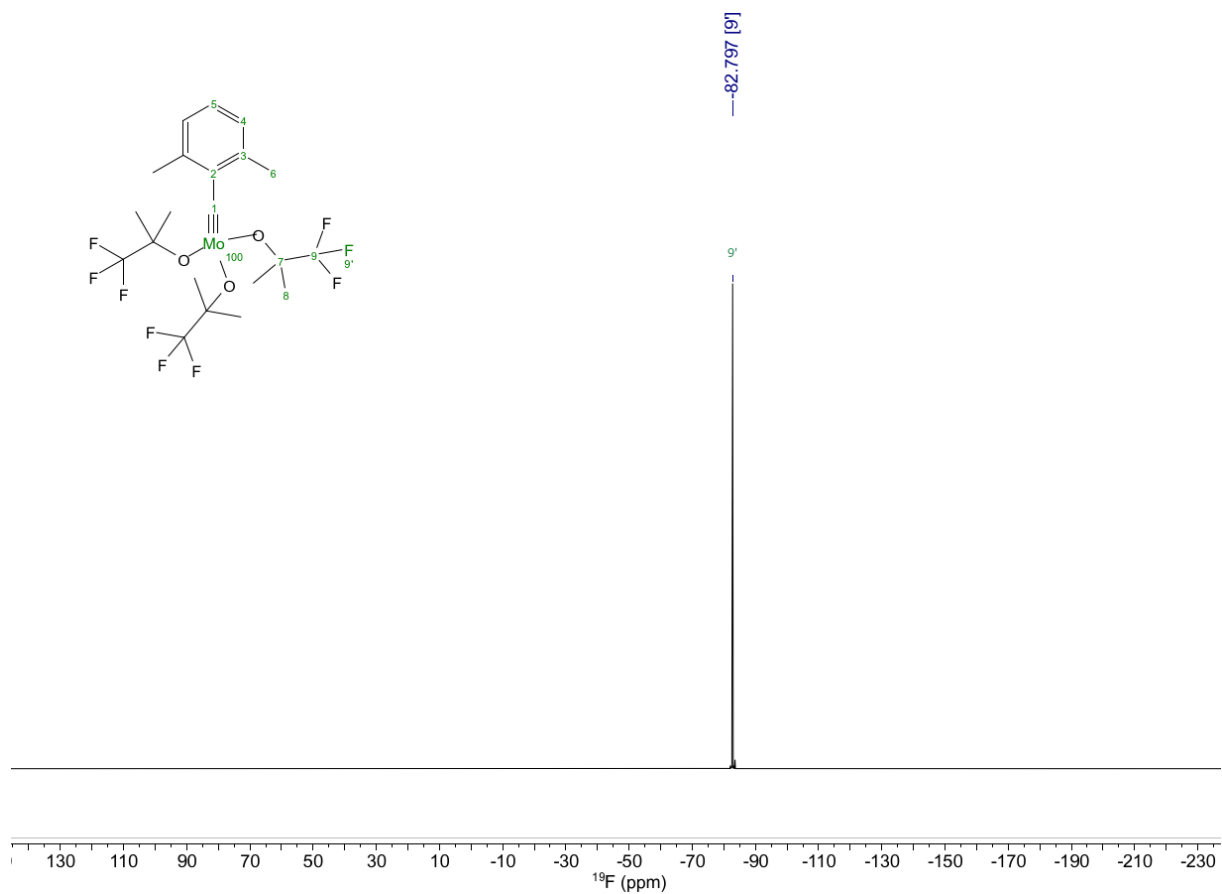


Figure S8. <sup>19</sup>F NMR spectrum of Complex **1<sub>F3</sub>**, 282 MHz, [D<sub>8</sub>]-toluene, ≈95% pure (see text)

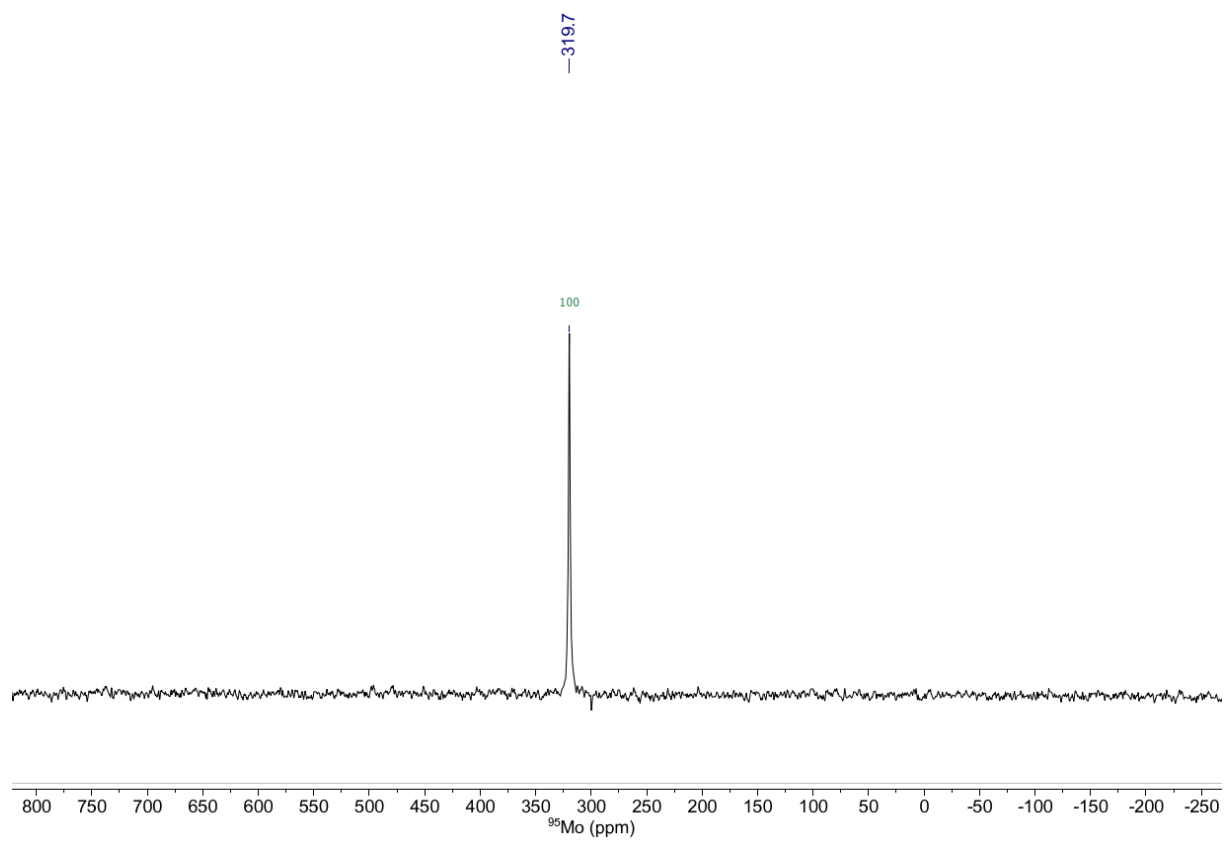


Figure S9.  $^{95}\text{Mo}$  NMR spectrum of Complex **1F3**, 26 MHz,  $[\text{D}_8]$ -toluene,  $60^\circ\text{C}$



### S2.3. Complex **1F6**

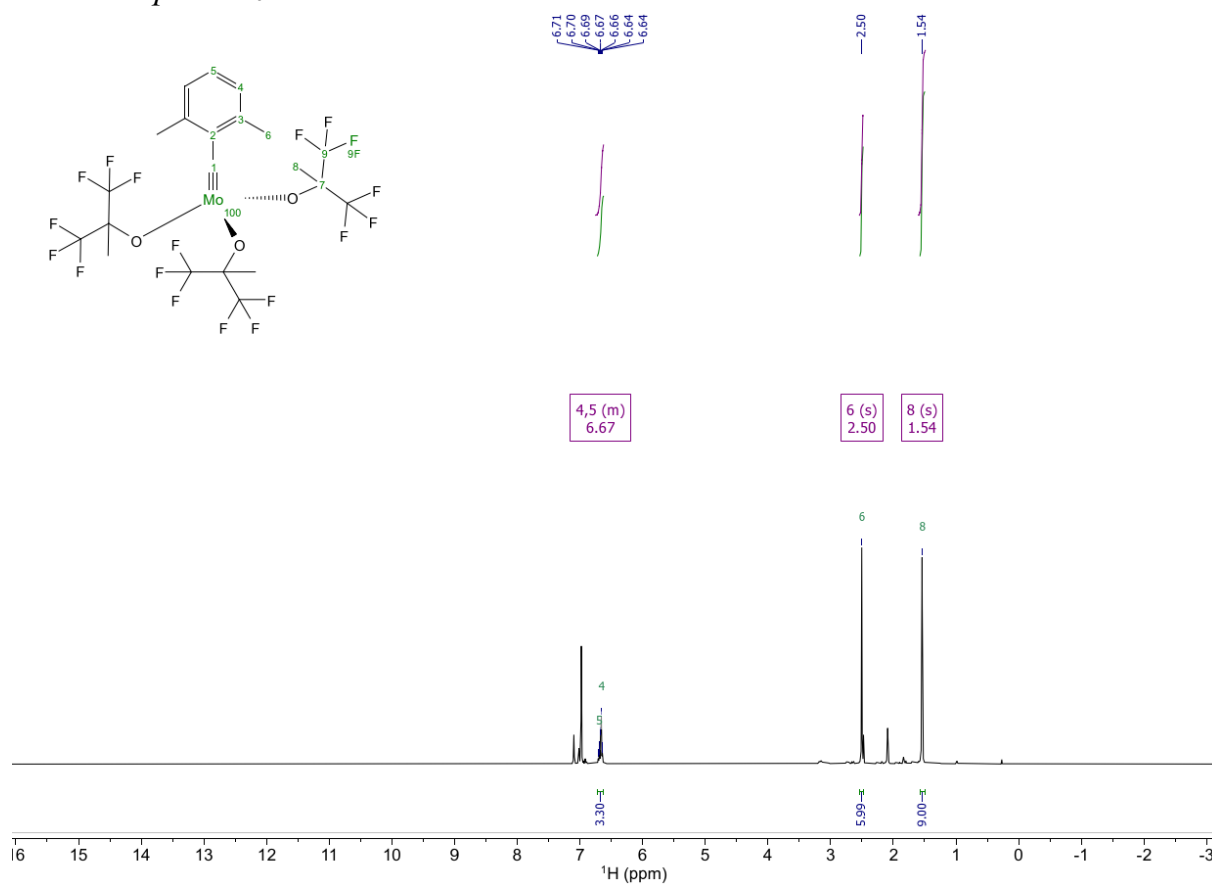


Figure S10.  $^1\text{H}$  NMR spectrum of Complex **1F6**, 600 MHz,  $[\text{D}_8]$ -toluene, 25°C (arbitrary numbering as shown)

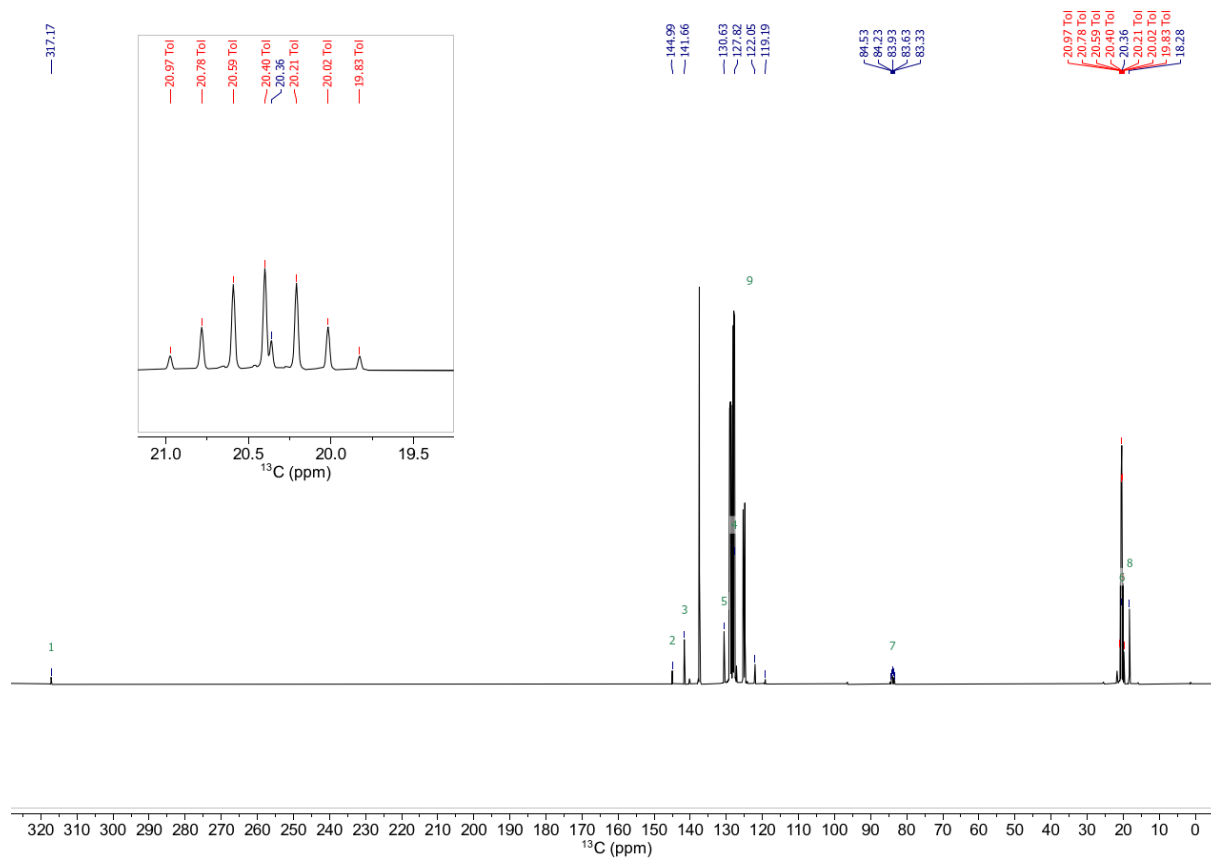


Figure S11.  $^{13}\text{C}$  NMR spectrum of Complex **1F6**, 151 MHz,  $[\text{D}_8]\text{-toluene}$ , 25°C (arbitrary numbering as above)

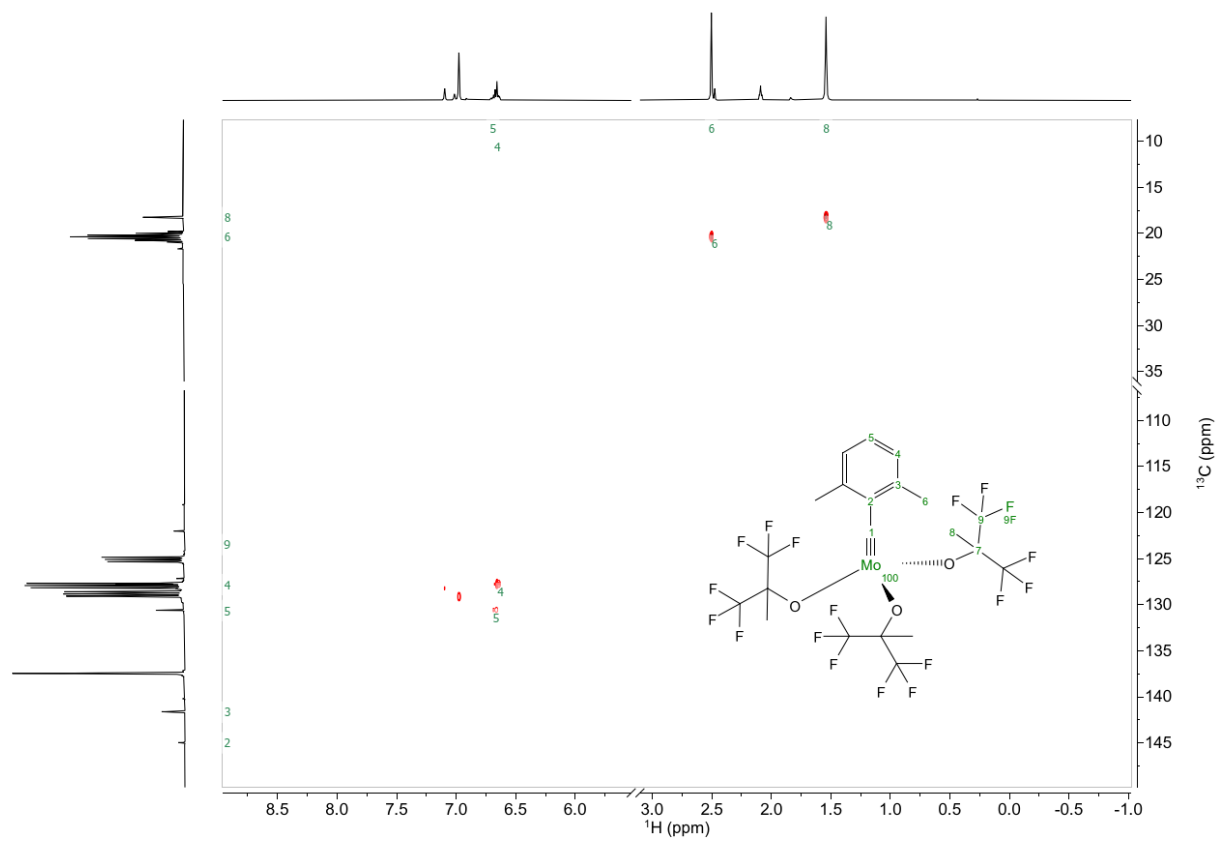


Figure S12.  $^1\text{H}$ - $^{13}\text{C}$ -HMQC spectrum of Complex  $1_{\text{F6}}$ , 600 MHz,  $[\text{D}_8]$ -toluene, 25°C (*arbitrary numbering as above*)

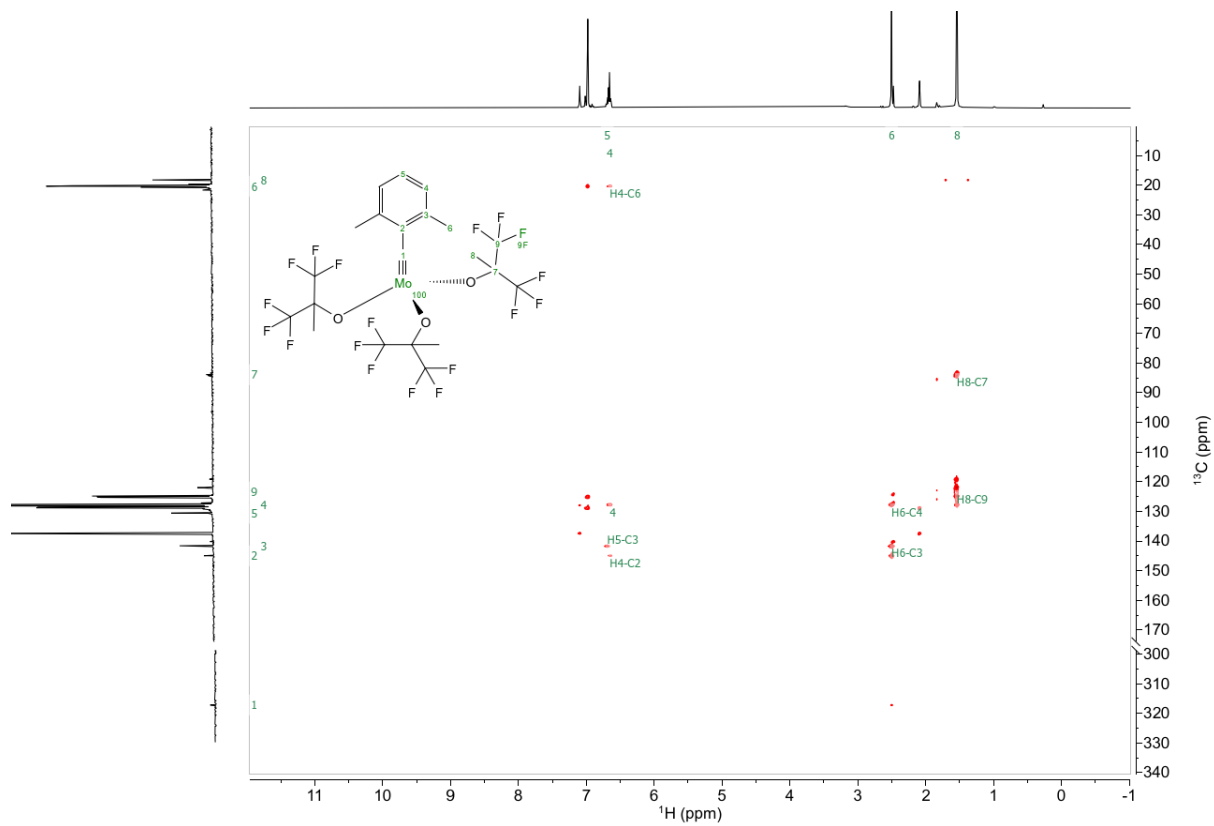


Figure S13.  $^1\text{H}$ - $^{13}\text{C}$ -HMBC spectrum of Complex  $1_{\text{F6}}$ , 600 MHz,  $[\text{D}_8]$ -toluene, 25°C (arbitrary numbering as above)

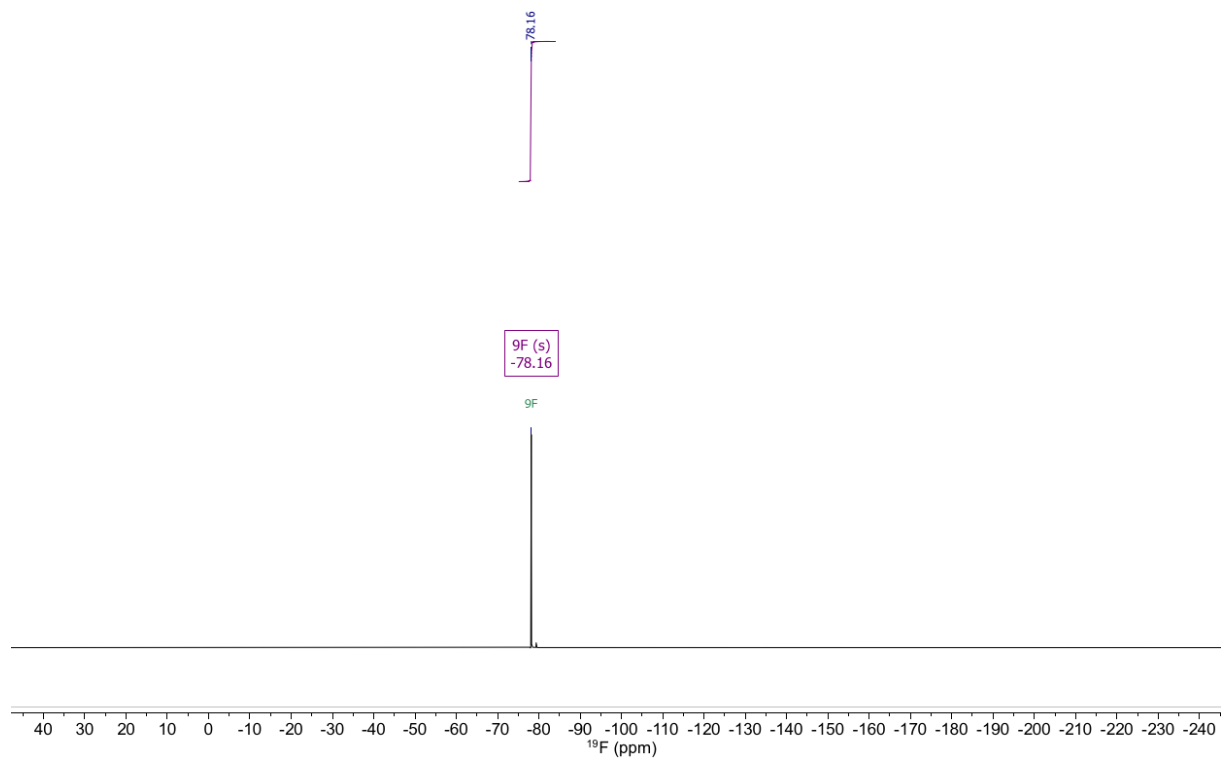


Figure S14.  $^{19}\text{F}$  NMR spectrum of Complex **1<sub>F6</sub>**, 282 MHz,  $[\text{D}_8]$ -toluene

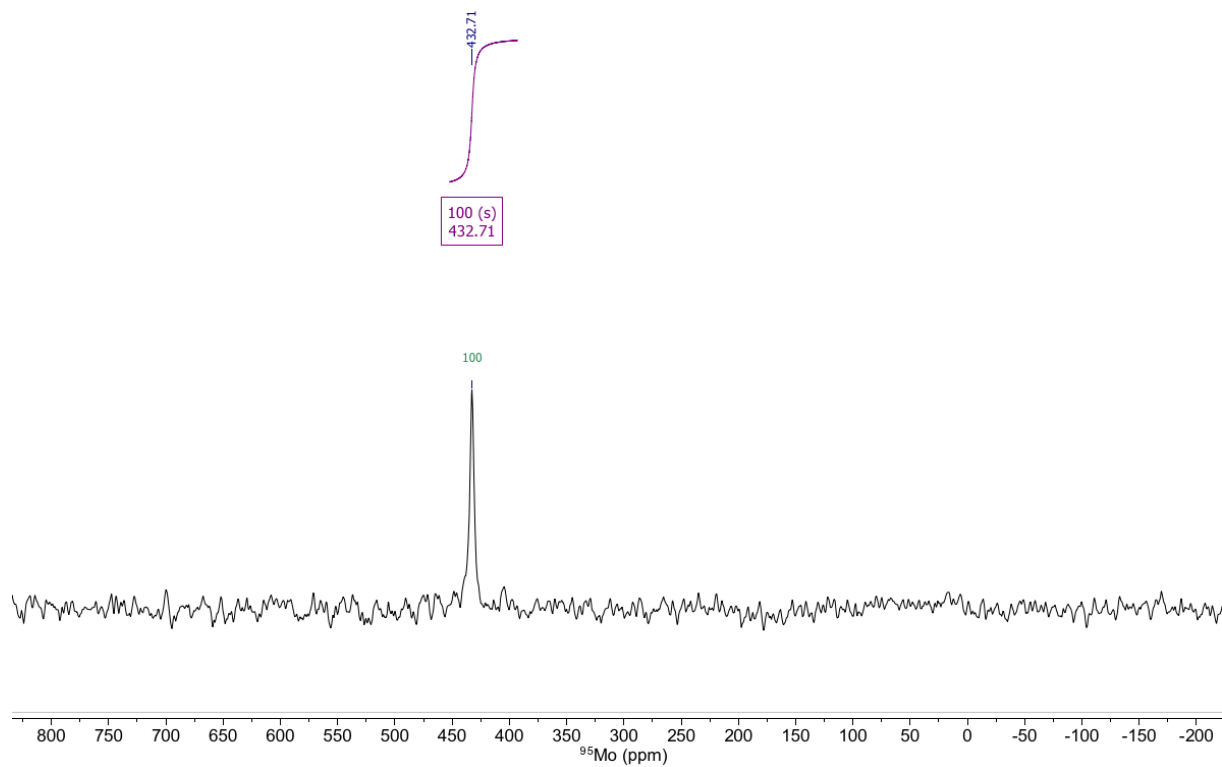


Figure S15.  $^{95}\text{Mo}$  NMR spectrum of Complex **1F6**, 26 MHz,  $[\text{D}_8]$ -toluene,  $60^\circ\text{C}$

## S2.4. Complex 1F9

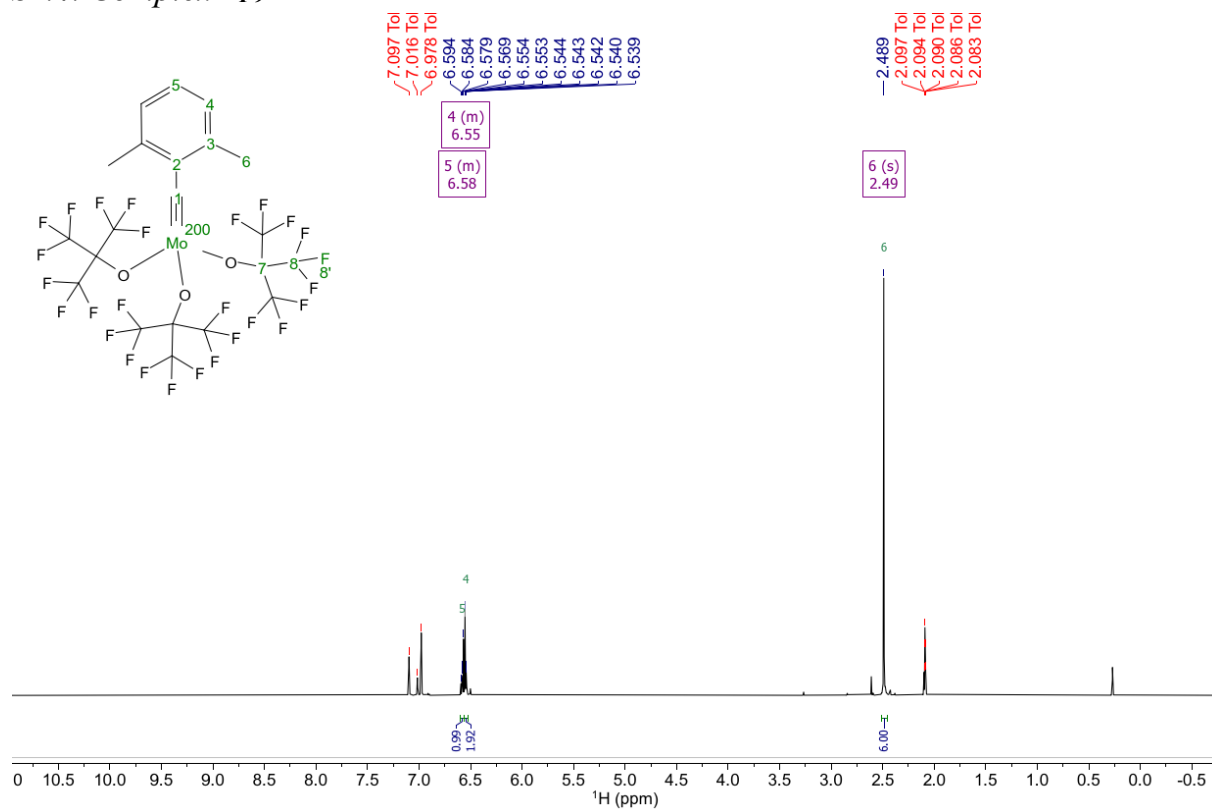


Figure S16.  $^1\text{H}$  NMR spectrum of Complex **1F9**, 600 MHz,  $[\text{D}_8]$ -toluene,  $25^\circ\text{C}$  (arbitrary numbering as shown)

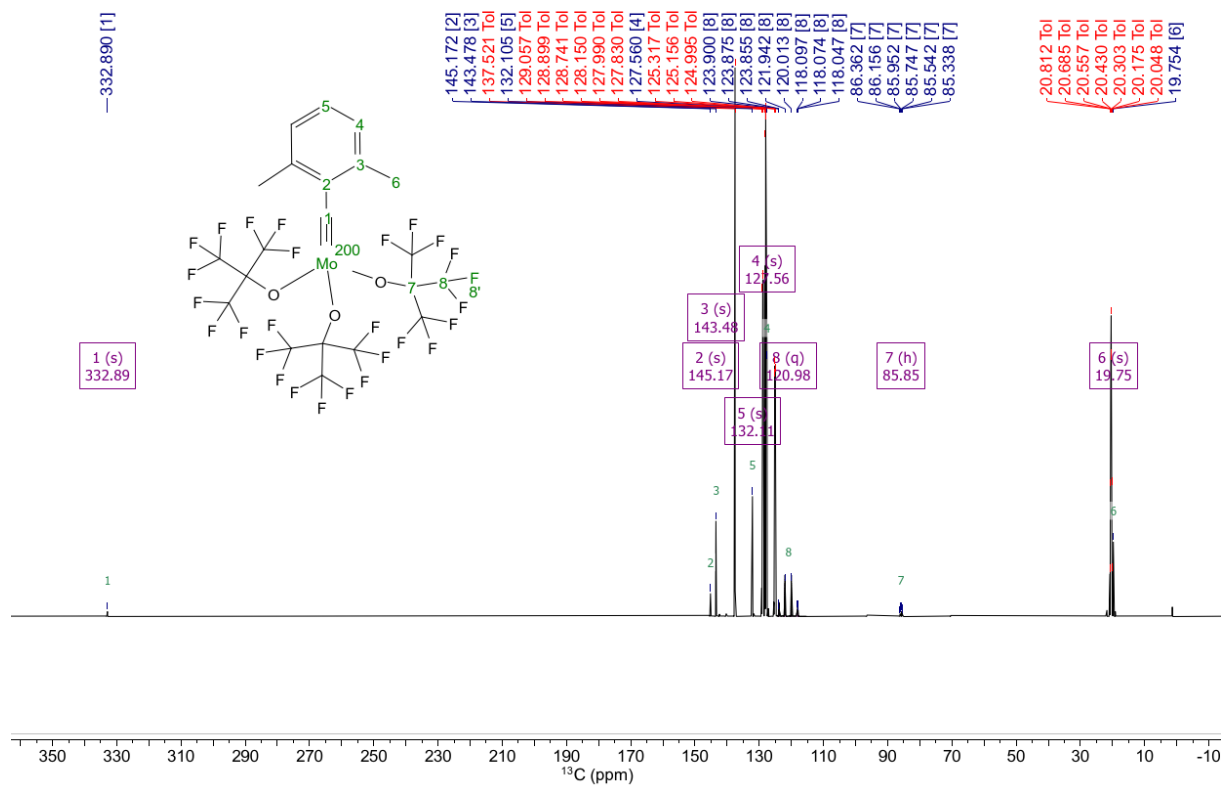


Figure S17.  $^{13}\text{C}$  NMR spectrum of Complex 1F9, 151 MHz,  $[\text{D}_8]$ -toluene, 25°C (*arbitrary numbering as above*)



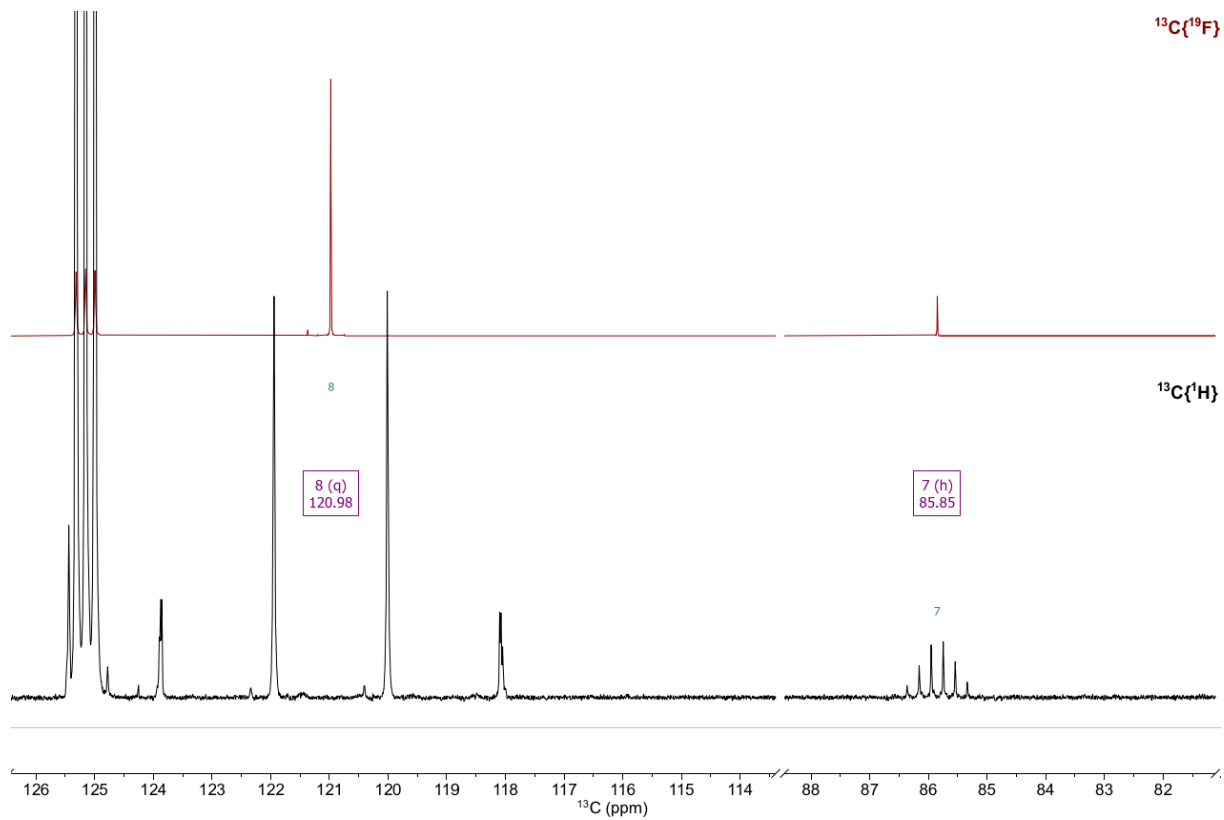


Figure S18.  $^{13}\text{C}$  NMR spectrum of Complex **1F9**, 151 MHz,  $[\text{D}_8]$ -toluene, 25°C (excerpts)

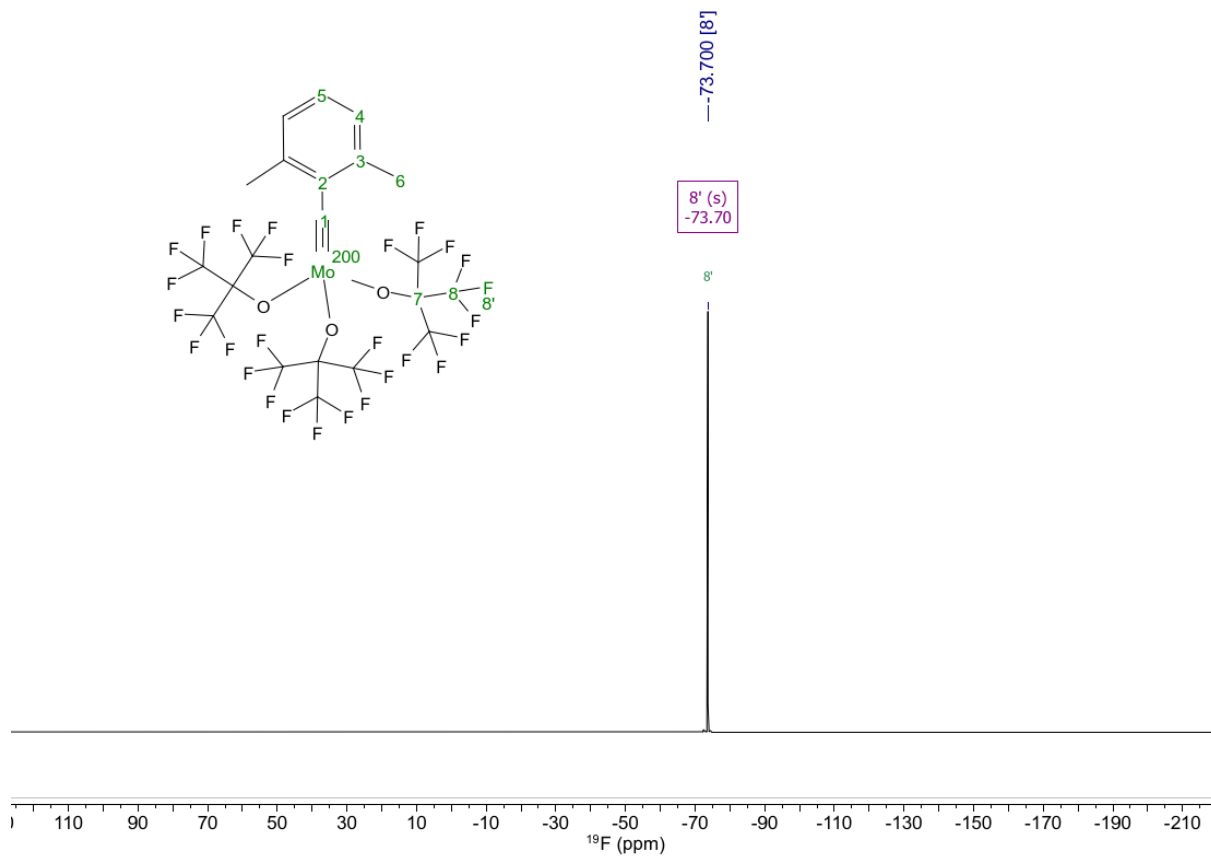


Figure S19.  $^{19}\text{F}$  NMR spectrum of Complex  $\mathbf{1F9}$ , 565 MHz,  $[\text{D}_8]$ -toluene

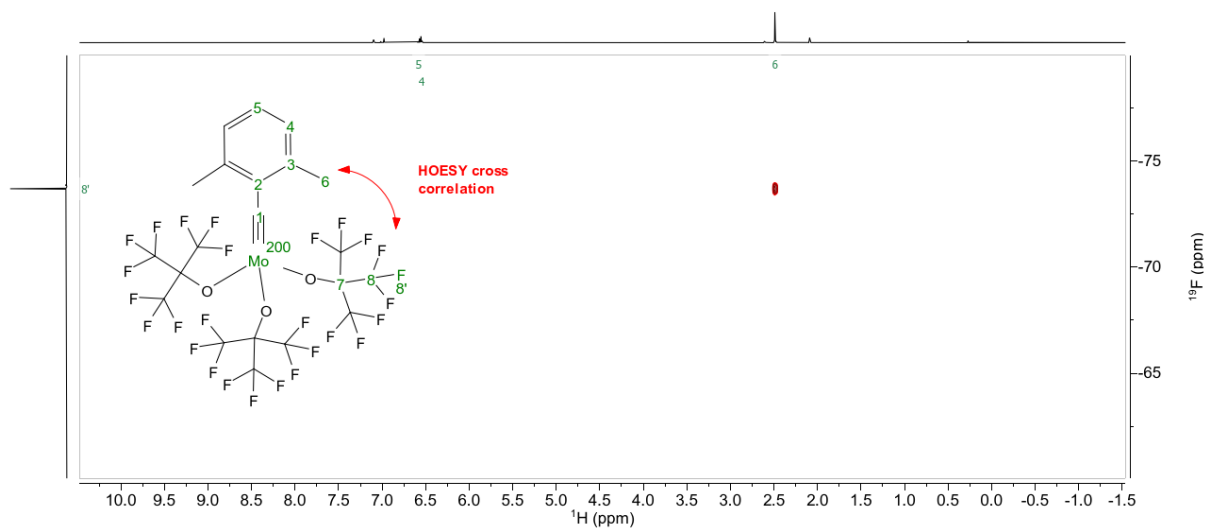


Figure S20.  $^1\text{H}$ ,  $^{19}\text{F}$  NOESY spectrum of Complex  $\mathbf{1F9}$ , 500 MHz,  $[\text{D}_8]$ -toluene

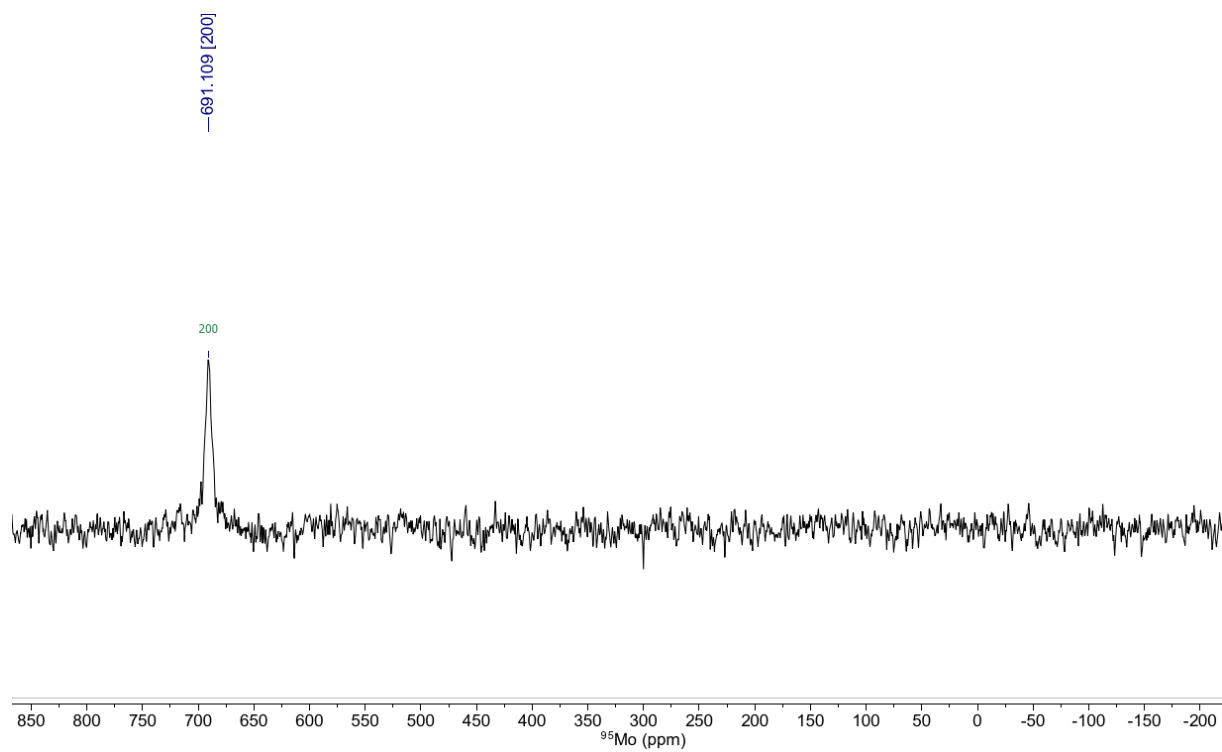


Figure S21.  $^{95}\text{Mo}$  NMR spectrum of Complex **1F9**, 26 MHz,  $[\text{D}_8]$ -toluene, 60°C

S2.5. Complex **2<sub>Ph</sub>**

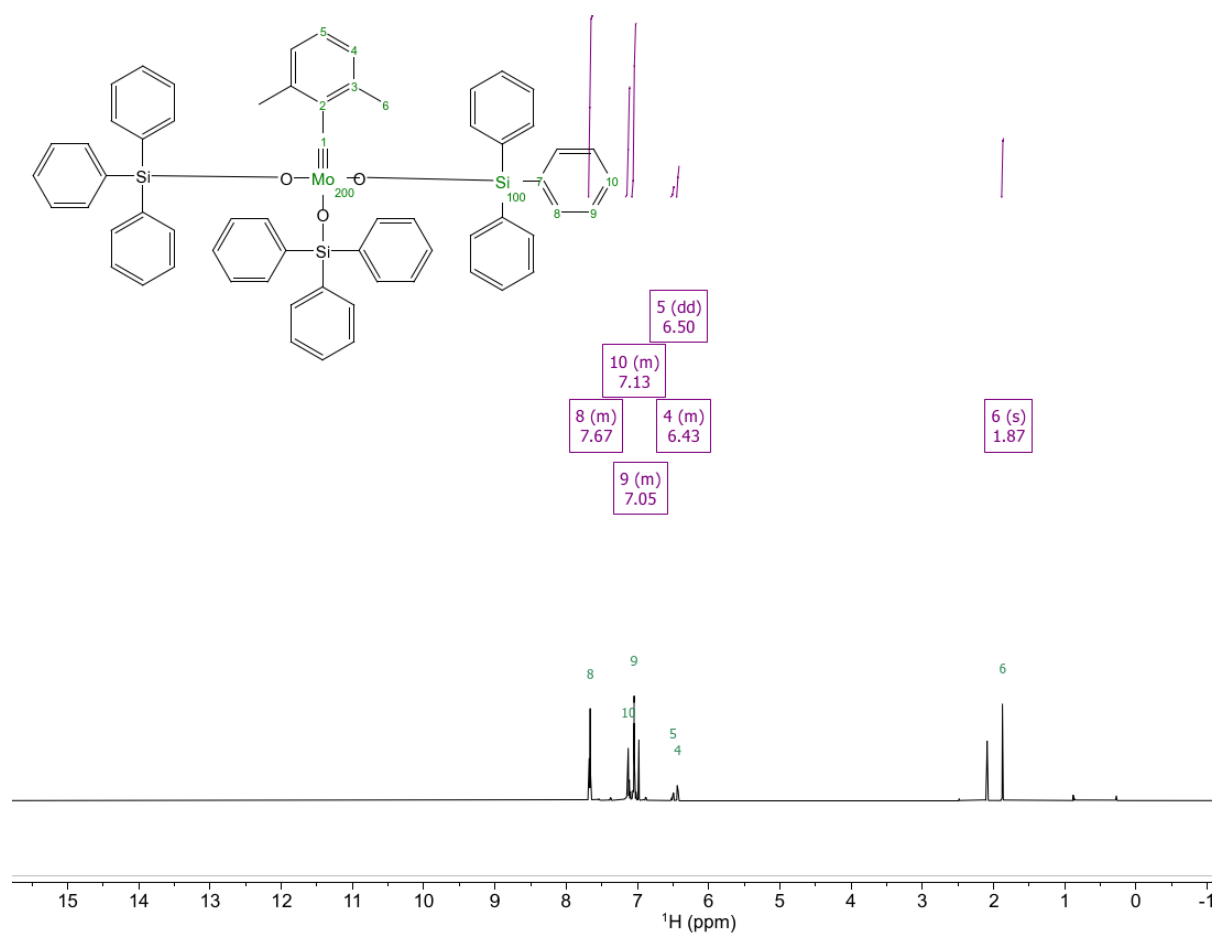


Figure S22. <sup>1</sup>H NMR spectrum of Complex **2<sub>Ph</sub>**, 600 MHz, [D<sub>8</sub>]-toluene, 25°C (*arbitrary numbering as shown*)

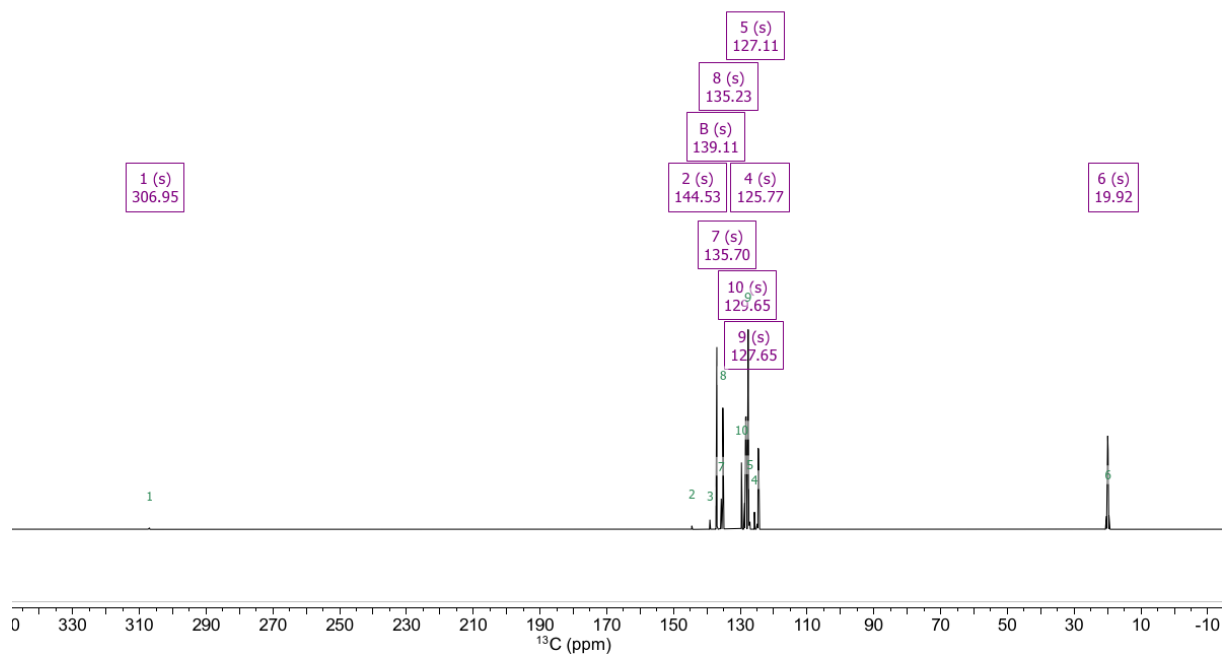


Figure S23.  $^{13}\text{C}$  NMR spectrum of Complex **2Ph**, 600 MHz,  $[\text{D}_8]$ -toluene, 25°C (*arbitrary numbering as above*)

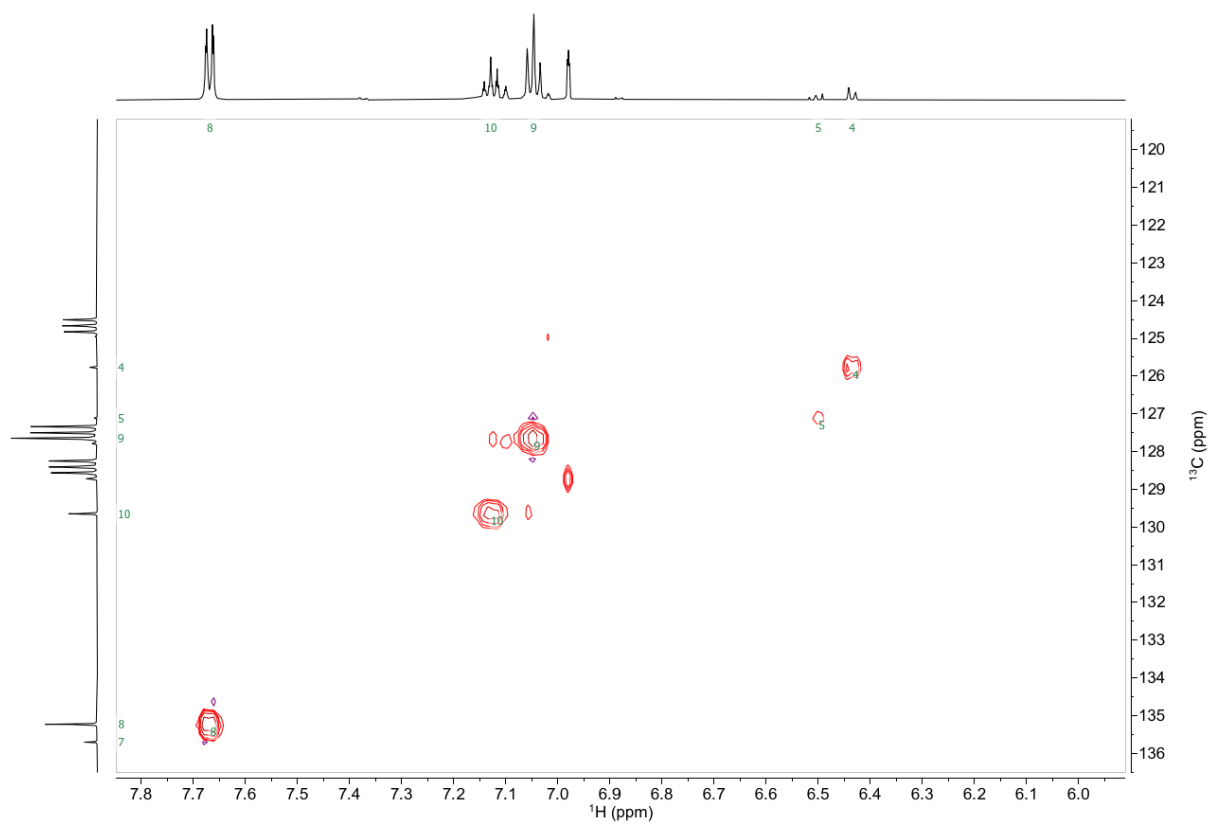


Figure S24.  $^1\text{H}$ - $^{13}\text{C}$ -HSQC spectrum of Complex **2<sub>Ph</sub>**, 600 MHz,  $[\text{D}_8]$ -toluene, 25°C (*arbitrary numbering as above*)

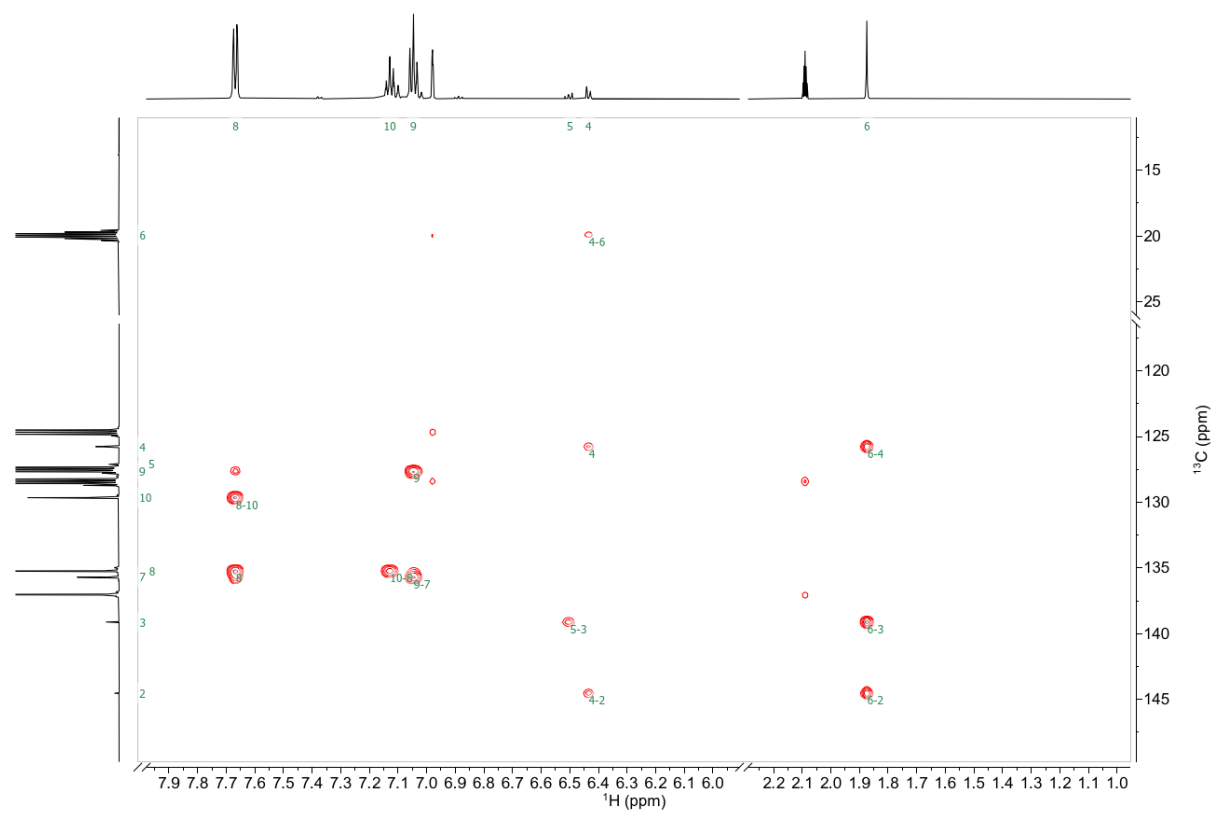


Figure S25.  $^1\text{H}$ - $^{13}\text{C}$ -HMBC spectrum of Complex **2<sub>Ph</sub>**, 600 MHz,  $[\text{D}_8]$ -toluene, 25°C (*arbitrary numbering as above*)

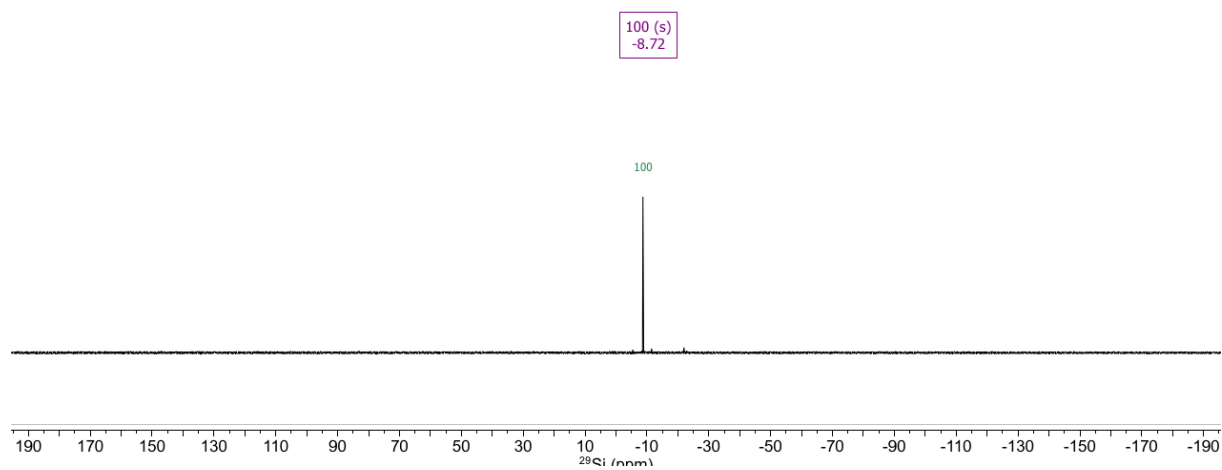


Figure S26.  $^{29}\text{Si}$  NMR spectrum of Complex **2<sub>Ph</sub>**, 79 MHz,  $[\text{D}_8]$ -toluene, 25°C

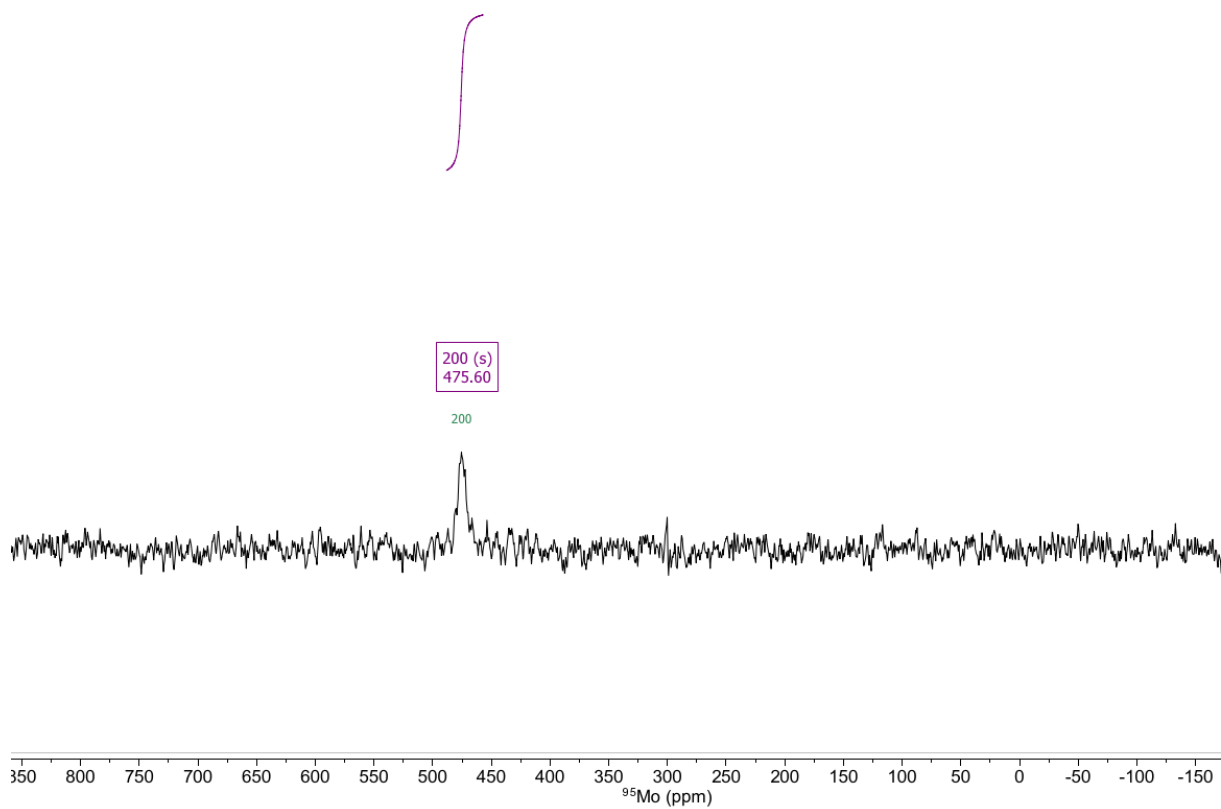


Figure S27.  $^{95}\text{Mo}$  NMR spectrum of Complex **2<sub>Ph</sub>**, 26 MHz,  $[\text{D}_8]$ -toluene, 60°C



## S2.6. Complex $3_{Ph}$

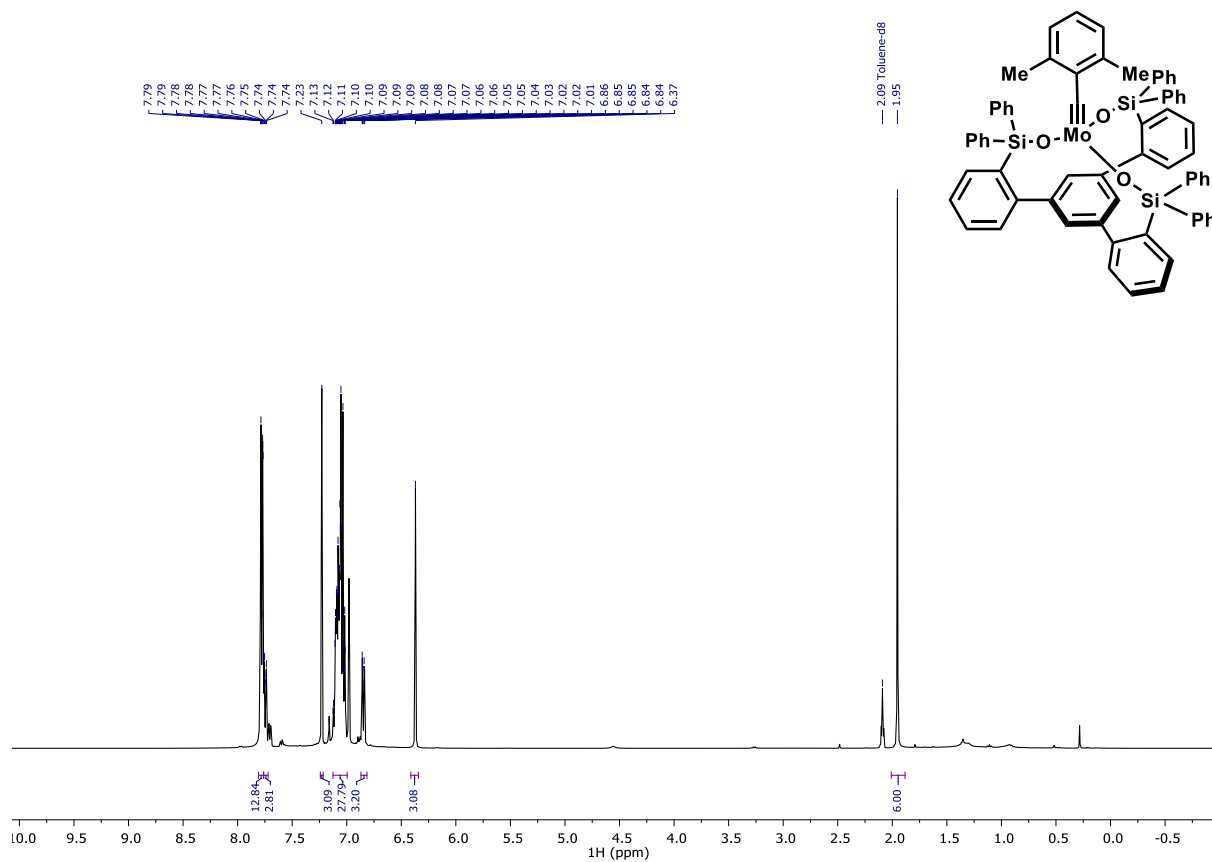


Figure S28.  $^1\text{H}$  NMR spectrum of Complex  $3_{Ph}$ , 400 MHz,  $[\text{D}_8]$ -toluene,  $25^\circ\text{C}$

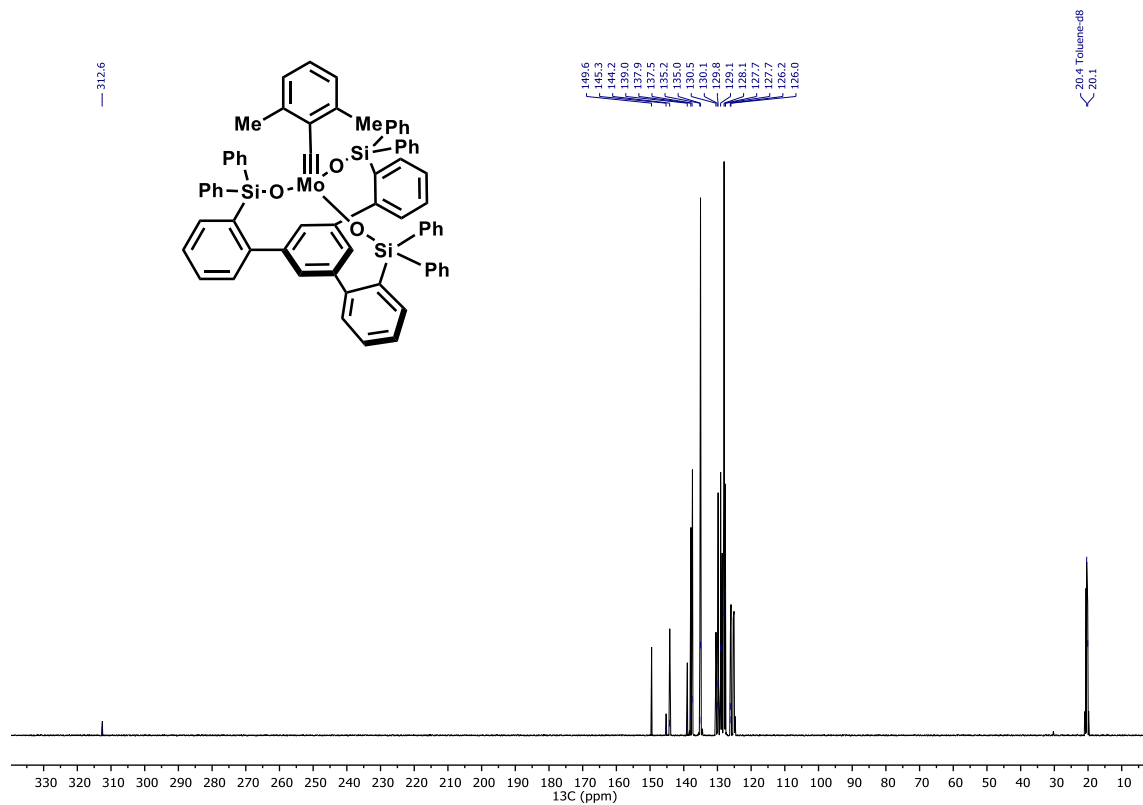


Figure S29. <sup>13</sup>C NMR spectrum of Complex **3<sub>Ph</sub>**, 101 MHz, [D<sub>8</sub>]-toluene, 25°C

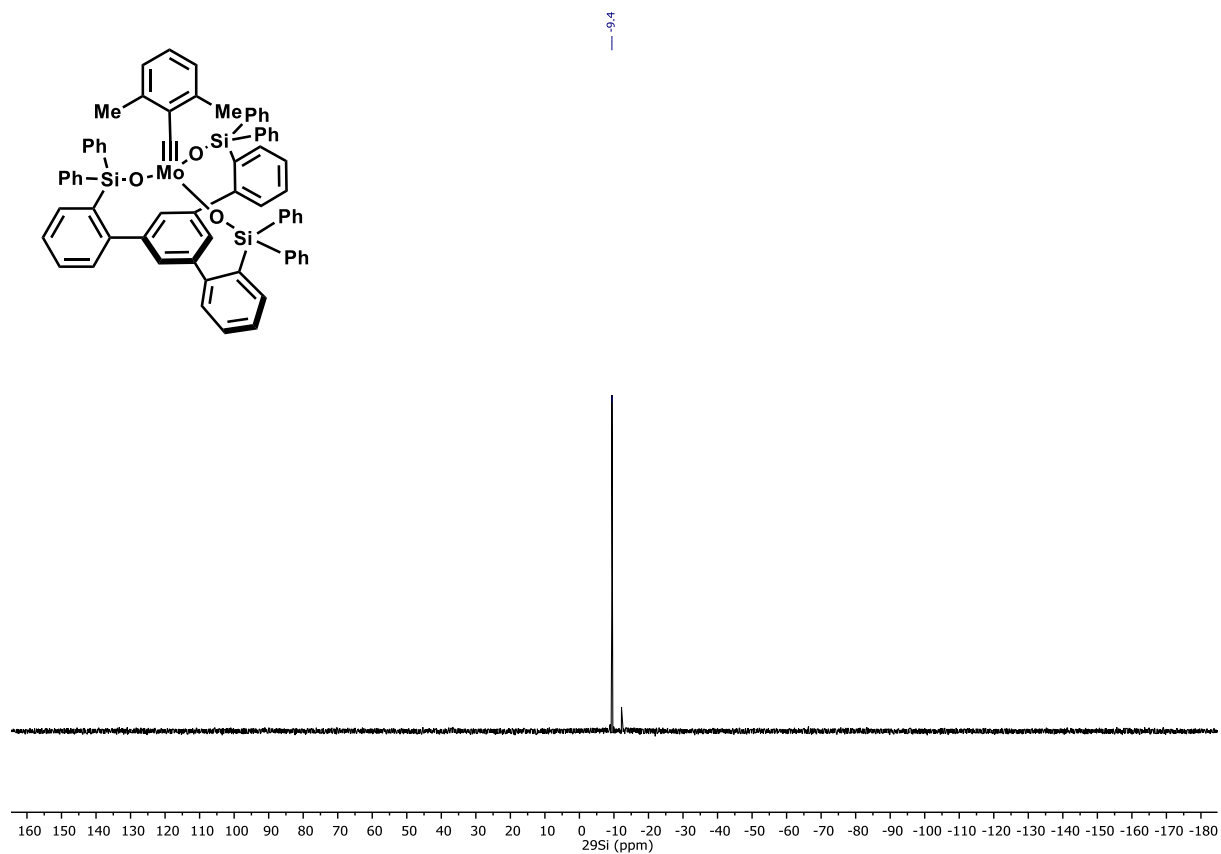


Figure S30. <sup>29</sup>Si NMR spectrum of Complex **3<sub>Ph</sub>**, 79 MHz, [D<sub>8</sub>]-toluene, 25°C

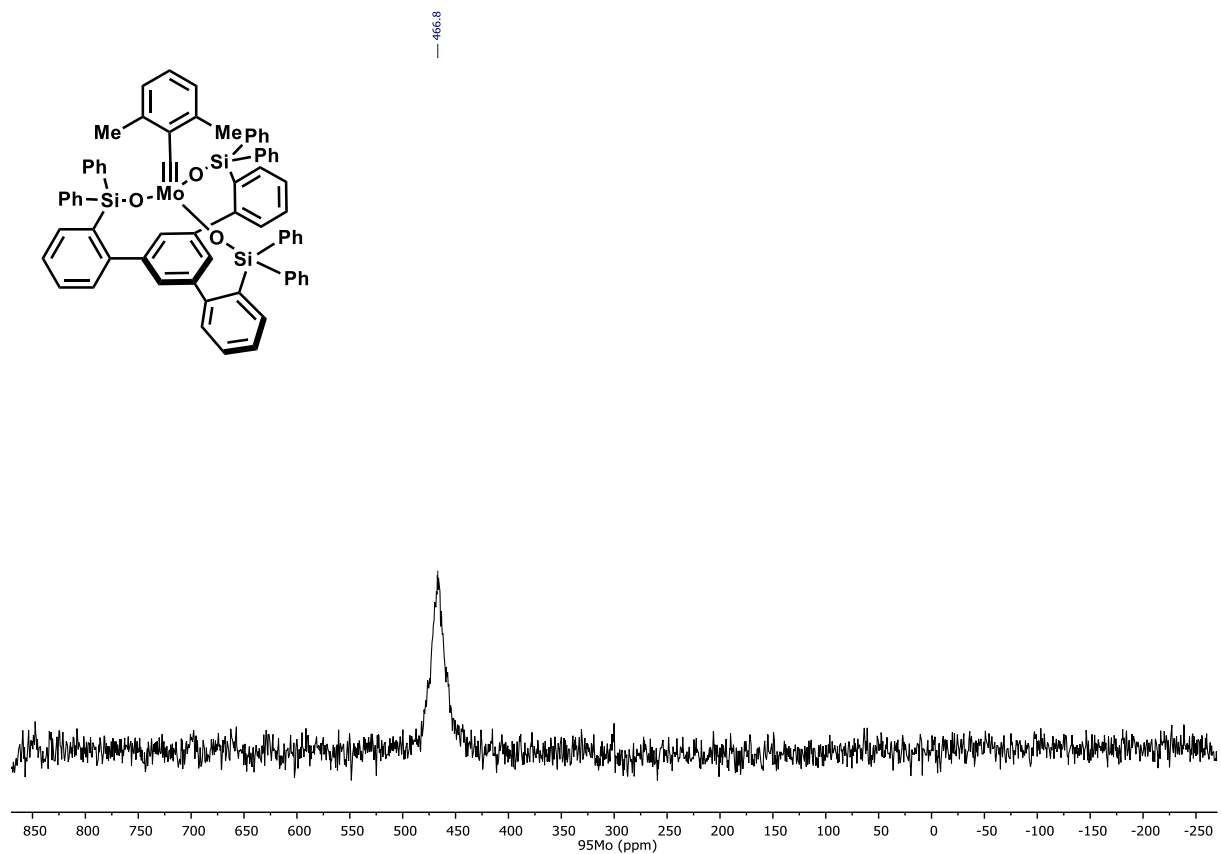


Figure S31. <sup>95</sup>Mo NMR spectrum of Complex **3<sub>Ph</sub>**, 26 MHz, [D<sub>8</sub>]-toluene, 60°C

S2.7. Complex  $3_{Et}$

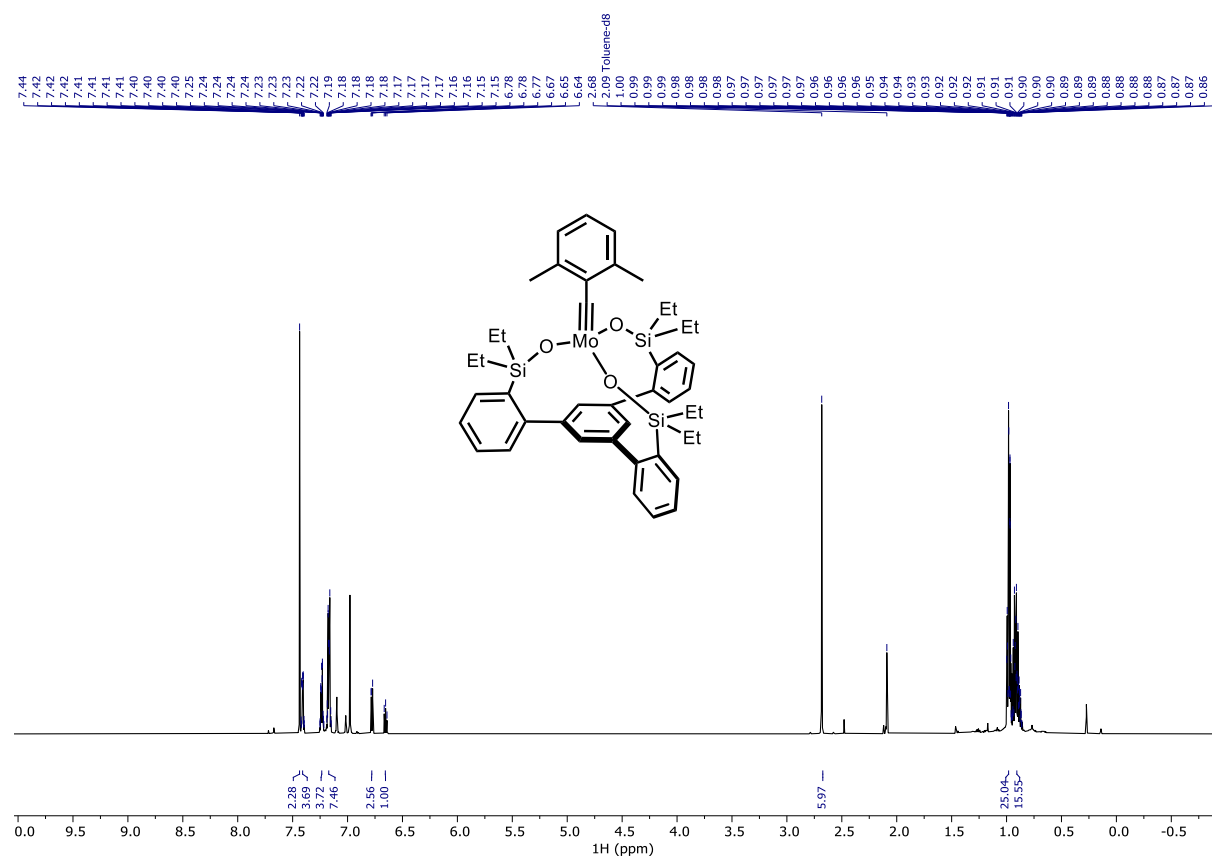


Figure S32.  $^1\text{H}$  NMR spectrum of Complex  $3_{Et}$ ,  $[\text{D}_8]\text{-toluene}$ ,  $25^\circ\text{C}$

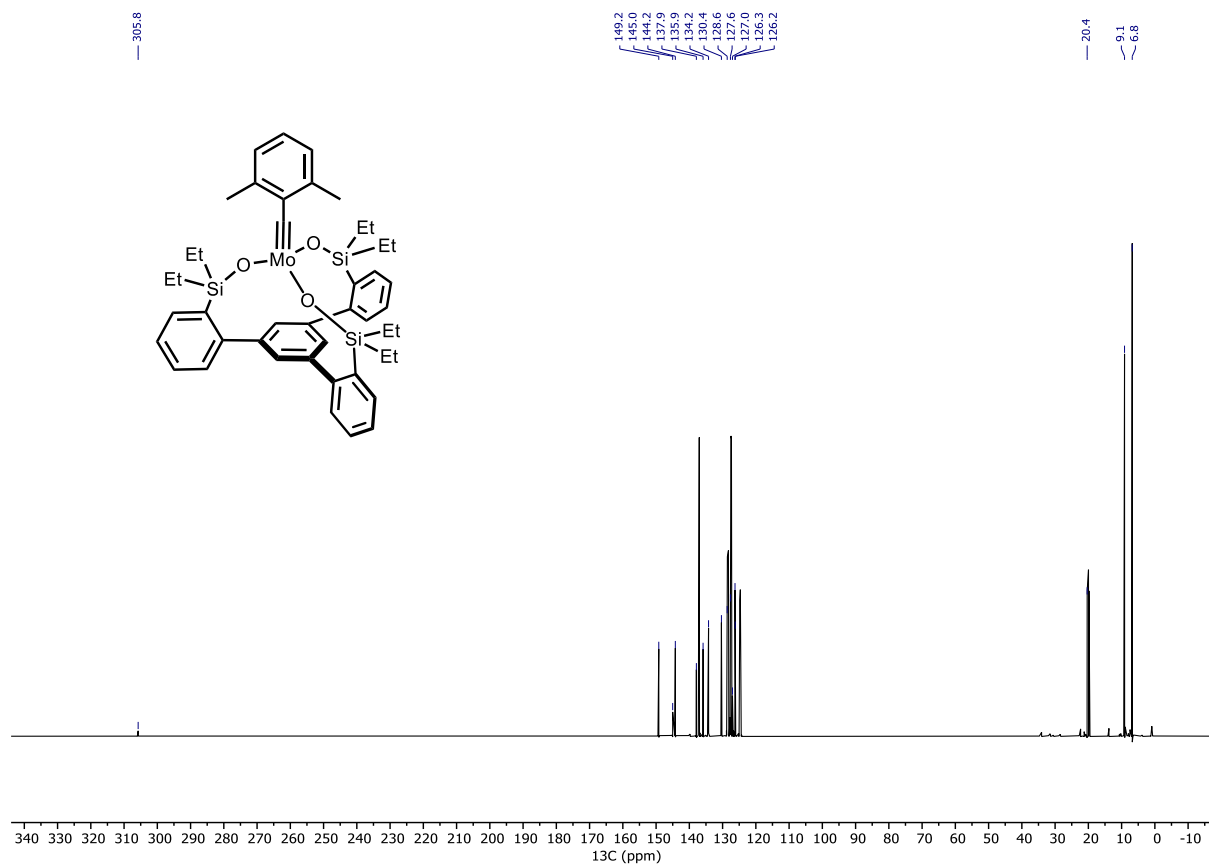


Figure S33. <sup>13</sup>C NMR spectrum of Complex **3**<sub>Et</sub>, [D<sub>8</sub>]-toluene, 25°C

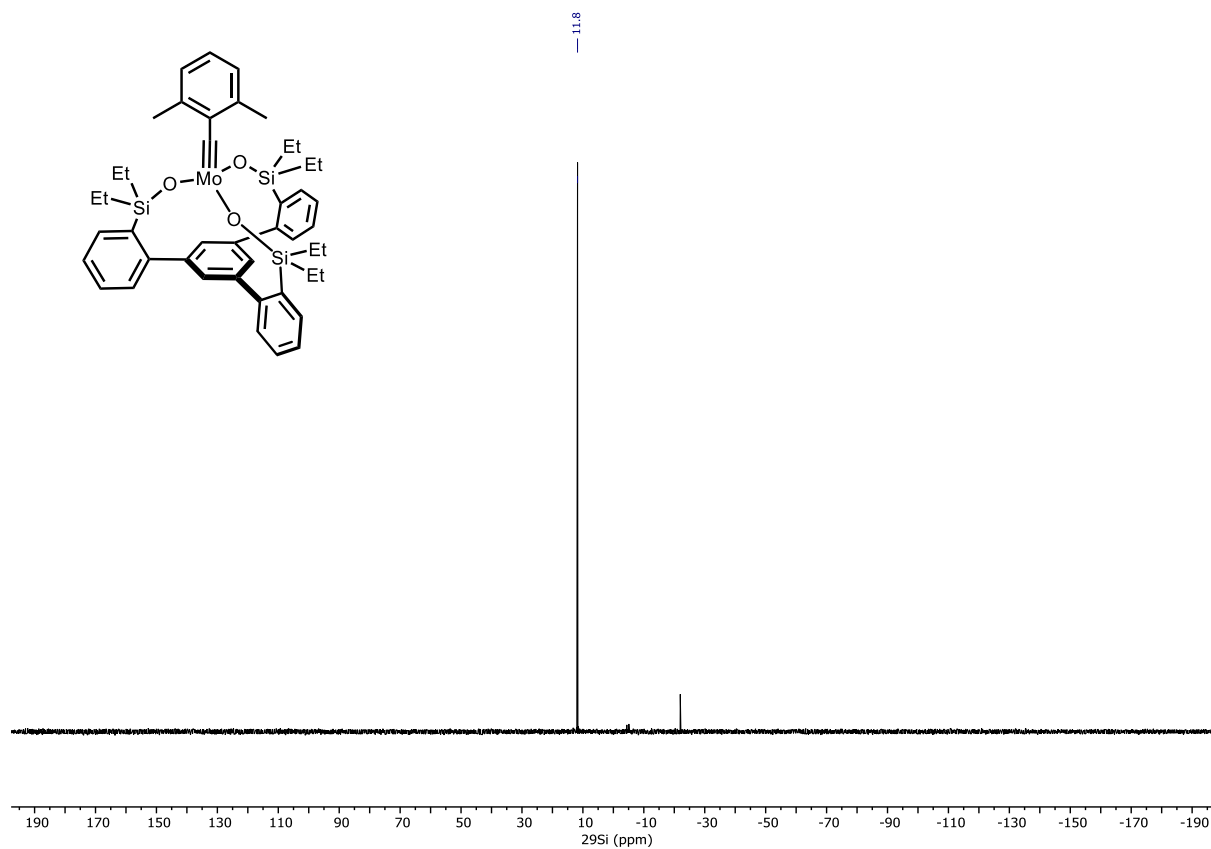


Figure S34. <sup>29</sup>Si NMR spectrum of Complex **3**<sub>Et</sub>, [D<sub>8</sub>]-toluene, 25°C

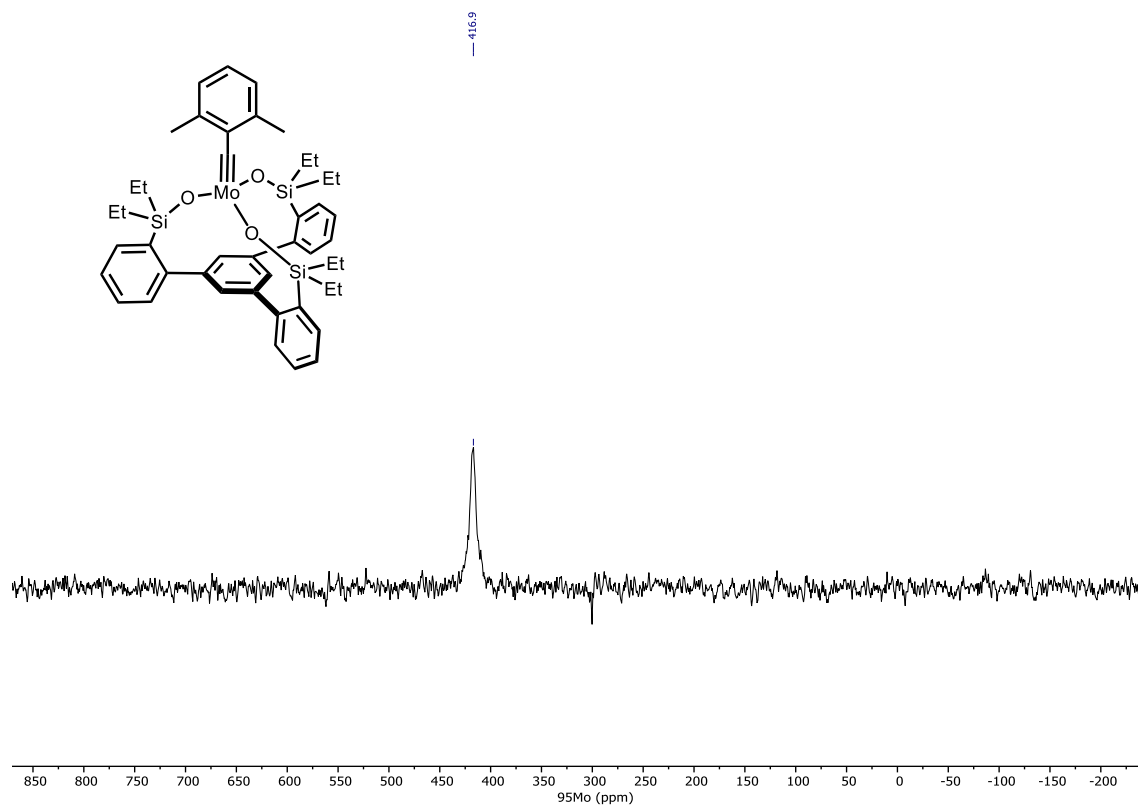
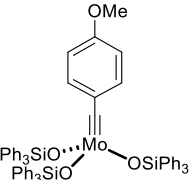
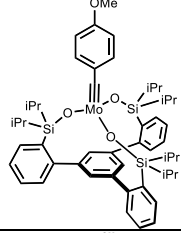
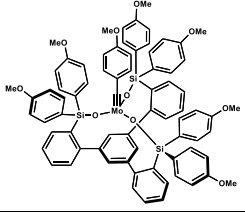
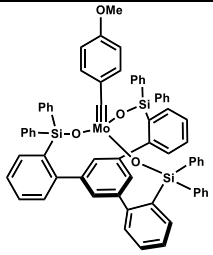
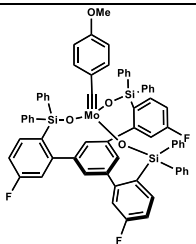


Figure S35. <sup>95</sup>Mo NMR spectrum of Complex **3<sub>Et</sub>**, [D<sub>8</sub>]-toluene, 60°C



## S2.8. Summary of Solution NMR data.

Table S2.1. Solution NMR data for Mo alkylidynes shown in Figure 1a of main text.

Compound	Solution <sup>95</sup> Mo isotropic chemical shift (ppm) <sup>a</sup>	Solution <sup>13</sup> C isotropic chemical shift (ppm) <sup>b</sup>	Solvent	Reference
<b>1F0</b>	259	297.1	C <sub>6</sub> D <sub>6</sub> ( <sup>13</sup> C); d <sub>8</sub> -toluene ( <sup>95</sup> Mo)	Ref. 2, this work
<b>1F3</b>	320	306.7	d <sub>8</sub> -toluene	This work
<b>1F6</b>	433	317.2	d <sub>8</sub> -toluene	This work
<b>1F9</b>	691	332.9	d <sub>8</sub> -toluene	This work
<b>2Ph</b>	475	306.9	d <sub>8</sub> -toluene	Ref. 3, this work
<b>3Ph</b>	467	312.2	d <sub>8</sub> -toluene	Ref. 2, this work
<b>3Et</b>	417	300.4	d <sub>8</sub> -toluene	Ref. 4, this work
	397	300.5	d <sub>8</sub> -toluene	Complex 1 in Ref. 21
	358	303.3	d <sub>8</sub> -toluene	Complex 1d in Ref. 2
	414	309.3	d <sub>8</sub> -toluene	Complex 1c in Ref. 2
	419	310.4	d <sub>8</sub> -toluene	Complex 1a in Ref. 2
	434	311.4	d <sub>8</sub> -toluene	Complex 1b in Ref. 2

### S3. Solid-state $^{95}\text{Mo}$ NMR analyses

#### S3.1. Experimental $^{95}\text{Mo}$ solid-state NMR spectra.

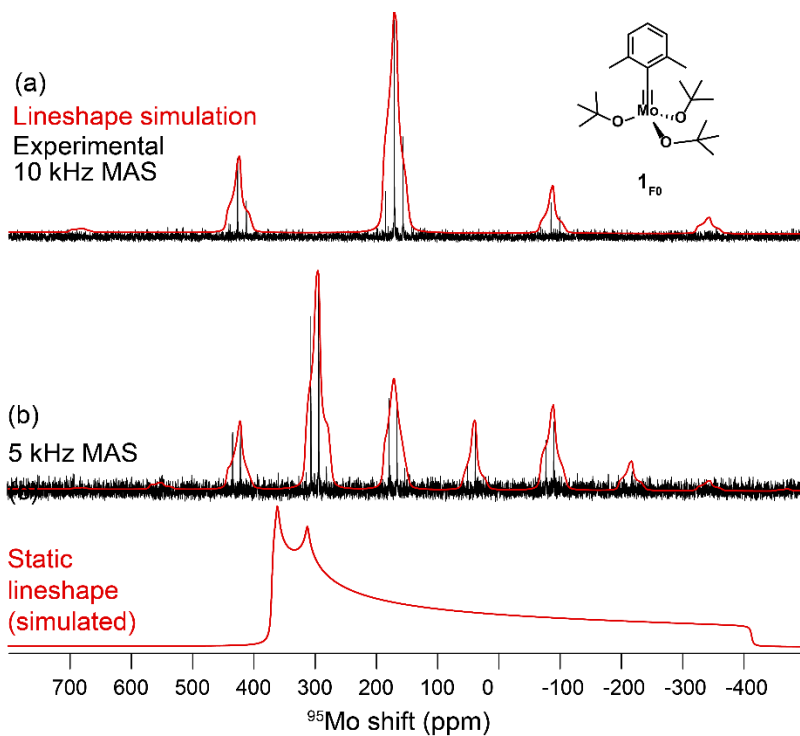


Figure S36. Experimental (black)  $^{95}\text{Mo}$  QCPMG-MAS NMR spectra of Complex  $1_{\text{F0}}$  (inset) along with simulated lineshapes (red) generated using the parameters shown in Table S2. Spectra were acquired at 100 K, 14.1 T, and at (a) 10 kHz MAS or (b) 5 kHz MAS.

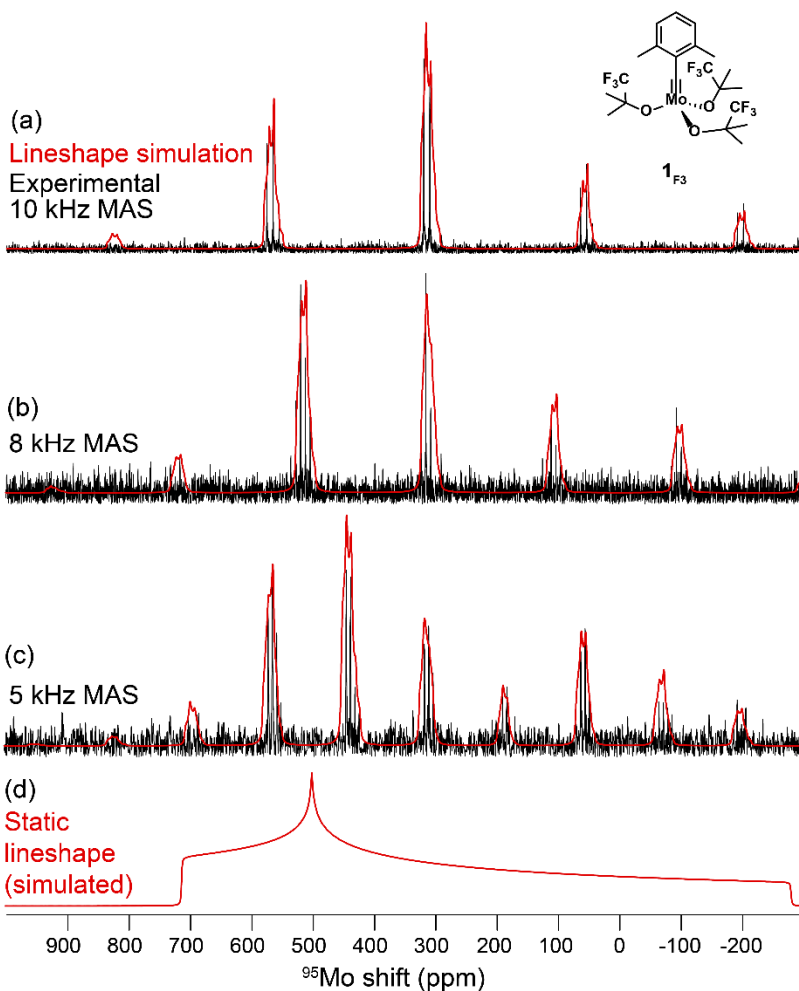


Figure S37. Experimental (black) <sup>95</sup>Mo QCPMG-MAS NMR spectra of Complex **1<sub>F3</sub>** (inset) along with simulated lineshapes (red) generated using the parameters provided in Table S2. Spectra were obtained at 100 K, 14.1 T, and at (a) 10 kHz MAS, (b) 8 kHz MAS, or (c) 5 kHz MAS.

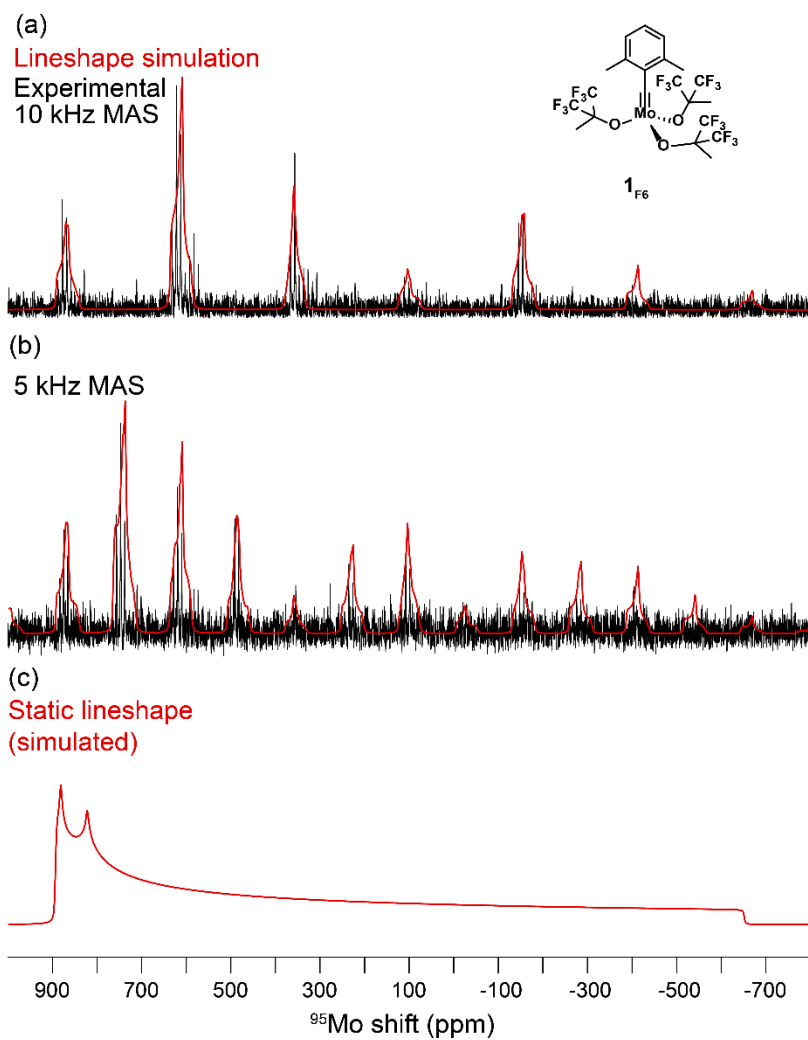


Figure S38. Experimental (black)  $^{95}\text{Mo}$  QCPMG-MAS NMR spectra of complex  $1_{F6}$  (inset) along with simulated lineshapes (red) generated using the parameters shown in Table S2. Spectra were obtained at 100 K, 14.1 T, and at (a) 10 kHz MAS or (b) 5 kHz MAS.

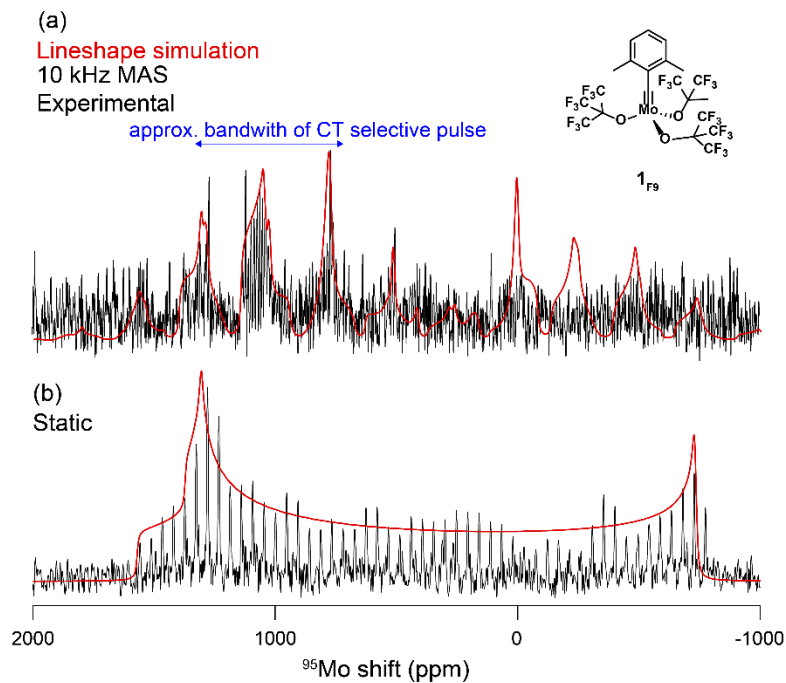


Figure S39. Experimental (black) <sup>95</sup>Mo QCPMG-MAS NMR spectra of complex **1<sub>F9</sub>** (inset) along with simulated lineshapes (red) generated using the parameters provided in Table S2. Spectra were obtained at 100 K, 14.1 T, and at (a) 10 kHz MAS (b) under static conditions.

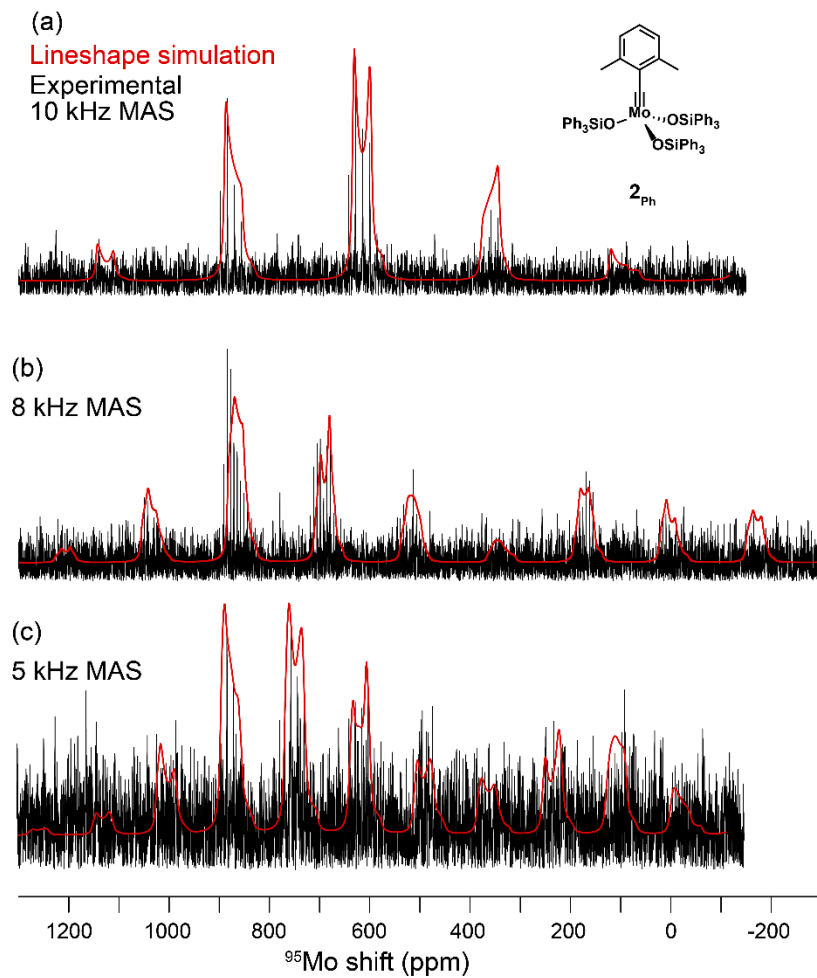


Figure S40. Experimental (black) <sup>95</sup>Mo QCPMG-MAS NMR spectra of Complex **2<sub>Ph</sub>** (inset) along with simulated lineshapes (red) generated using the parameters provided in Table S2. Spectra were obtained at 100 K, 14.1 T, and at (a) 10 kHz MAS, (b) 8 kHz MAS, or (c) 5 kHz MAS.

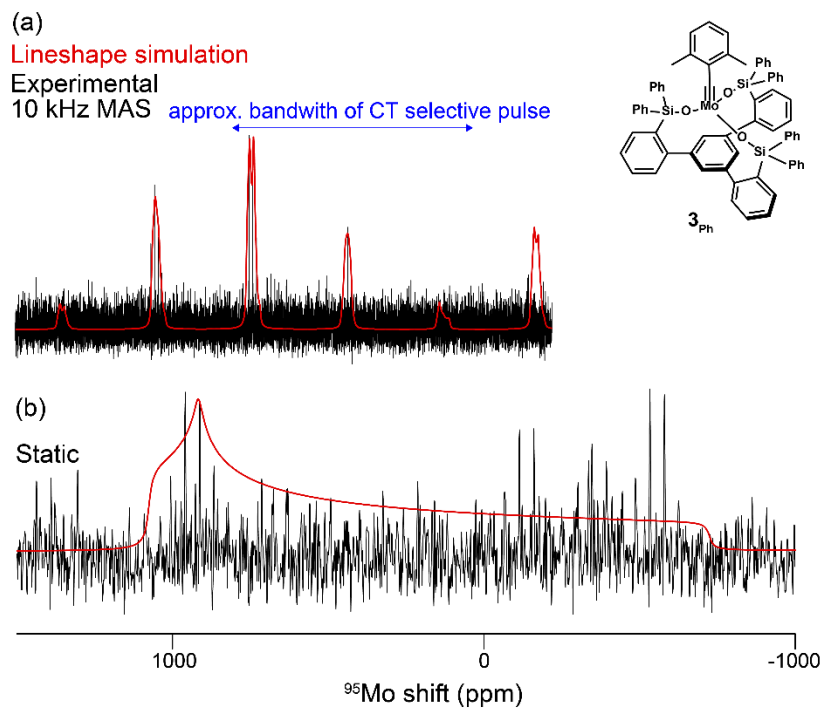


Figure S41. Experimental (black)  $^{95}\text{Mo}$  QCPMG-MAS NMR spectra of Complex  $3_{\text{Ph}}$  (inset) along with simulated lineshapes (red) generated using the parameters provided in Table S2. The spectra were obtained at 100 K, 14.1 T, and (a) 10 kHz MAS or (b) static conditions.

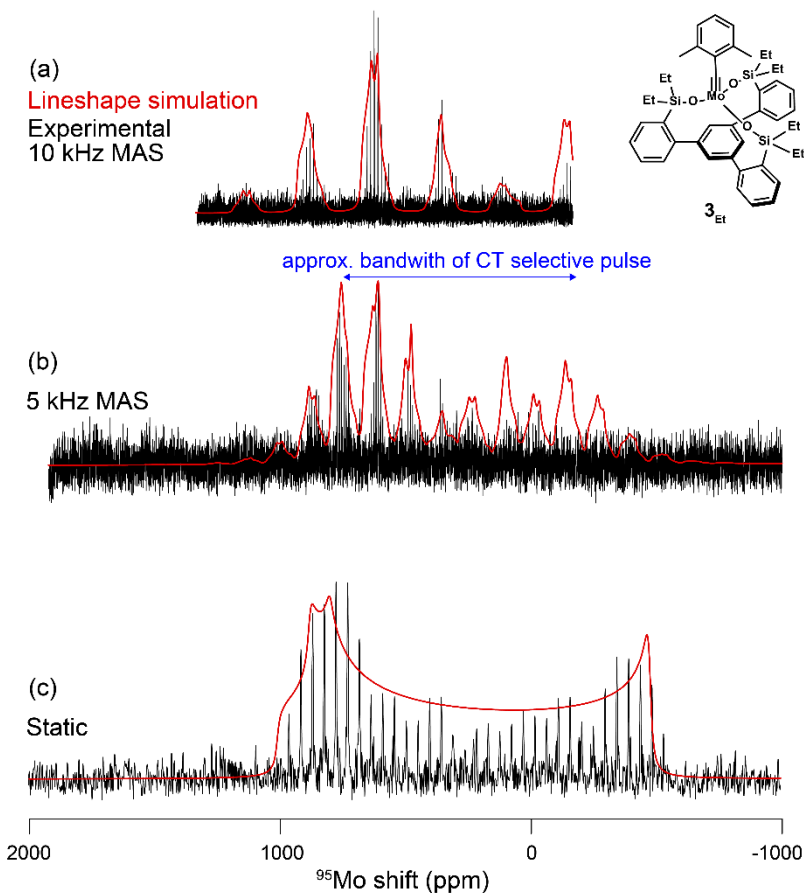


Figure S42. Experimental (black) <sup>95</sup>Mo QCPMG-MAS NMR spectra of Complex **3<sub>Et</sub>** (inset) along with simulated lineshapes (red) generated using the parameters provided in Table S2. Spectra were obtained at 100 K, 14.1 T, and at (a) 10 kHz MAS, (b) 5 kHz MAS, or (c) under static conditions.



### S3.2. Summary of $^{95}\text{Mo}$ solid-state NMR data.

Table S3.1. Solid-state  $^{95}\text{Mo}$  NMR parameters extracted from experimental spectra.

	$\delta_{\text{iso}}^{\text{a}}$	$\delta_{\text{CSA}}^{\text{b}}$	$\eta_{\text{CSA}}^{\text{c}}$	$C_{\text{Q}}^{\text{d}}$	$\eta_{\text{Q}}^{\text{e}}$	$\Omega^{\text{f}}$	$\kappa^{\text{g}}$	$\delta_{11}^{\text{h}}$	$\delta_{22}^{\text{h}}$	$\delta_{33}^{\text{h}}$	$\phi^{\text{i}}$	$\chi^{\text{i}}$	$\psi^{\text{i}}$	$\delta_{\text{perp}}^{\text{j}}$
<b>1<sub>F0</sub></b>	190	-475	0	2.0	0.8	715	1.0	425	425	-290	115	35	115	424
<b>1<sub>F3</sub></b>	330	-600	0.3	2.0	0.5	990	0.6	720	540	-270	115	15	115	630
<b>1<sub>F6</sub></b>	380	-1000	0.3	2.2	1.0	1500	1.0	880	880	-620	115	35	115	880
<b>1<sub>F9</sub></b>	610	-1400	0.0	4.5	0.8	2100	1.0	1310	1310	-790	115	5	115	1310
<b>2<sub>Ph</sub></b>	400	-1100	0.1	2.7	0.4	1705	0.9	1005	895	-700	115	0	115	950
<b>3<sub>Ph</sub></b>	435	-1100	0.1	2.5	1	1705	1.0	1040	930	-665	115	0	115	985
<b>3<sub>Et</sub></b>	380	-910	0.1	3.7	0.6	1410	0.9	880	790	-530	115	0	115	835

<sup>a</sup> Isotropic  $^{95}\text{Mo}$  chemical shift in ppm;  $\pm 10$  ppm  
<sup>b</sup> Reduced anisotropy of chemical shift tensor in Haerberlen convention in ppm;  $\pm 25$  ppm  
<sup>c</sup> Asymmetry of chemical shift tensor in Haerberlen convention;  $\pm 0.2$   
<sup>d</sup> Quadrupolar coupling constant in MHz, estimated  
<sup>e</sup> Asymmetry of efg tensor, estimated  
<sup>f</sup> Span of chemical shift tensor in Herzfeld-Berger convention in ppm;  $\pm 25$  ppm  
<sup>g</sup> Skew of chemical shift tensor in Herzfeld-Berger convention;  $\pm 0.2$  ppm  
<sup>h</sup> Principal components of chemical shift tensor in standard convention in ppm;  $\pm 25$  ppm  
<sup>i</sup> Euler angles in degrees, estimated  
<sup>j</sup>  $\delta_{\text{perp}} = (\delta_{11} + \delta_{22})/2$  in ppm;  $\pm 25$  ppm

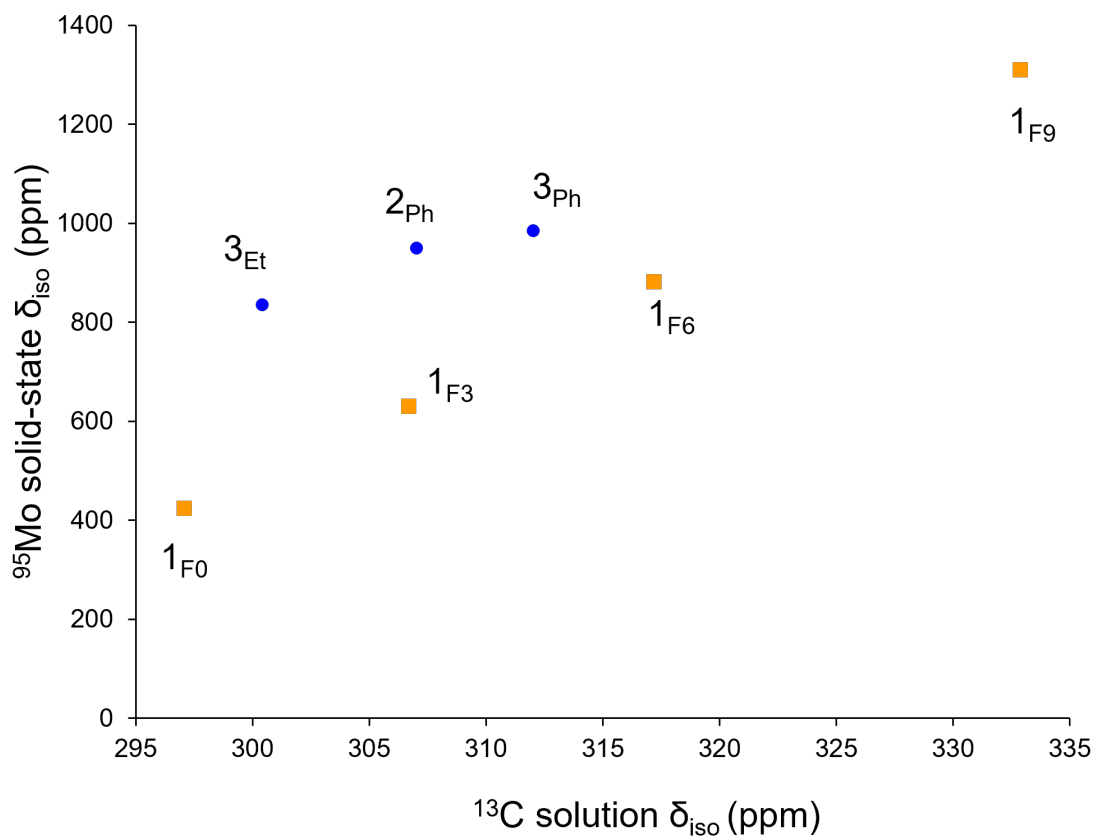


Figure S43. Plot of experimentally determined  $^{95}\text{Mo}$  isotropic chemical shifts  $\delta_{\text{iso}}$  against the  $^{13}\text{C}$   $\delta_{\text{iso}}$  of the alkylidyne carbon for (blue) the silanolate series and (orange) the alkoxide series.

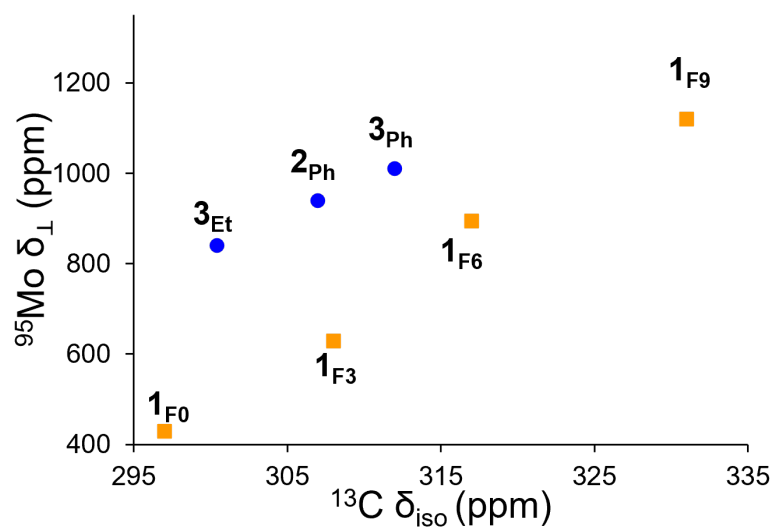


Figure S44. Plot of experimentally determined  $^{95}\text{Mo}$   $\delta_{\perp}$  against the  $^{13}\text{C}$   $\delta_{\text{iso}}$  of the alkylidyne carbon for (blue) the silanolate series and (orange) the alkoxide series.

## S4. DFT analyses

### S4.1. Summary of DFT calculations of $^{95}\text{Mo}$ NMR parameters.

Table S4.1. Results of DFT calculations of  $^{95}\text{Mo}$  NMR parameters

	$\sigma_{11}$ (ppm)	$\sigma_{22}$ (ppm)	$\sigma_{33}$ (ppm)	$\sigma_{\text{iso}}$ (ppm)	$\Omega$ (ppm) Calculated/ experimental	$ \kappa $ Calculated/ experimental	$ C_Q $ (MHz) Calculated/ experimental	$\eta_Q$ Calculated/ experimental
<b>1<sub>F0</sub></b>	-953	-842	-497	-764	455/715	0.5/1.0	1.7/2.0	0.3/0.8
<b>1<sub>F3</sub></b>	-1123	-1061	-367	-850	756/990	0.84/0.6	2.6/2.0	0.6/0.5
<b>1<sub>F6</sub></b>	-1416	-1221	-215	-951	1621/1500	0.65/1.0	4.0/2.2	0.95/1.0
<b>1<sub>F9</sub></b>	-1872	-1614	72	-1185	1800/2100	0.71/1.0	6.6/4.5	0.7/0.8
<b>2<sub>Ph</sub></b>	-1540	-1254	81	-904	1349/1705	0.83/0.9	4.6/2.7	0.4/0.4
<b>3<sub>Ph</sub></b>	-1461	-1348	111	-899	1512/1705	0.73/1.0	3.9/2.5	0.4/0.4
<b>3<sub>Et</sub></b>	-1475	-1269	37	-902	1201/1410	0.68/0.9	5.2/3.7	0.6/0.6

## S4.2. Benchmarking of DFT calculations.

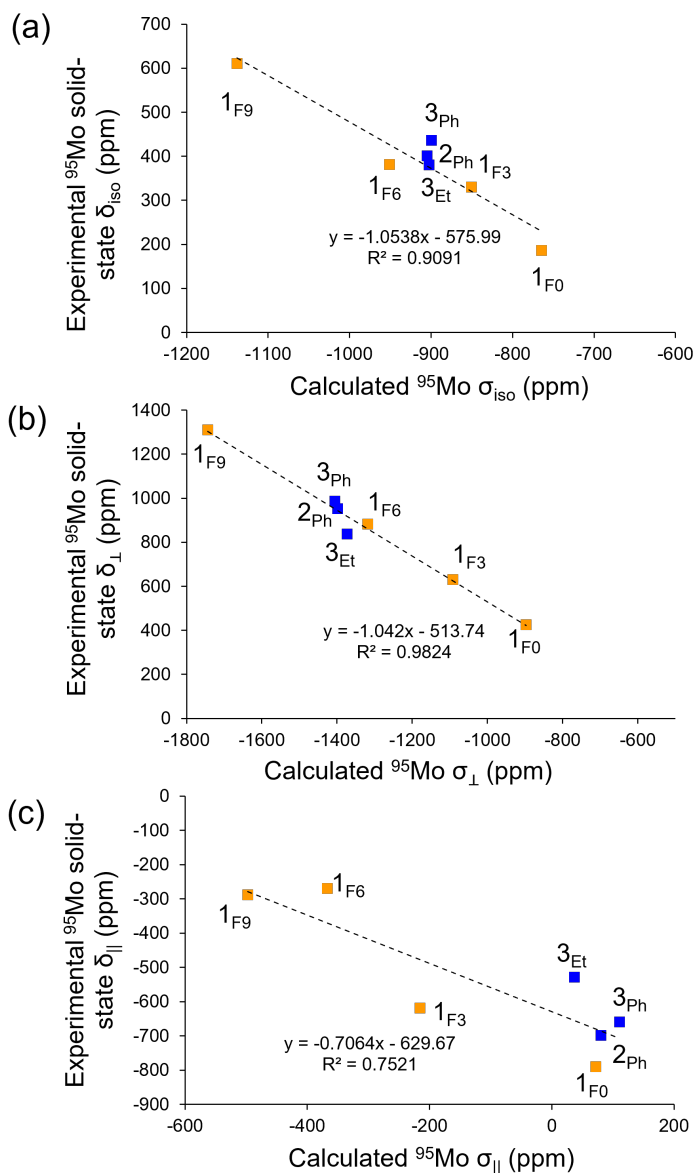


Figure S45. Benchmarking of DFT calculations of  $^{95}\text{Mo}$  chemical shift tensors. (a) Correlation of  $^{95}\text{Mo}$   $\delta_{\text{iso}}$  from experimental solid-state  $^{95}\text{Mo}$  NMR spectra plotted against calculated  $^{95}\text{Mo}$   $\sigma_{\text{iso}}$ . The dotted black line is a linear least squares regression. The overall linear agreement with regression slope close to 1 indicates good accuracy of the DFT calculations. Closer inspection of the individual chemical shift tensor components (b)  $\delta_{\perp} = (\delta_{11} + \delta_{22})/2$  reveal very good agreement between experimental  $\delta_{\perp}$  and calculated  $\sigma_{\perp}$ .

### S4.3. Orientations of chemical shielding tensors.

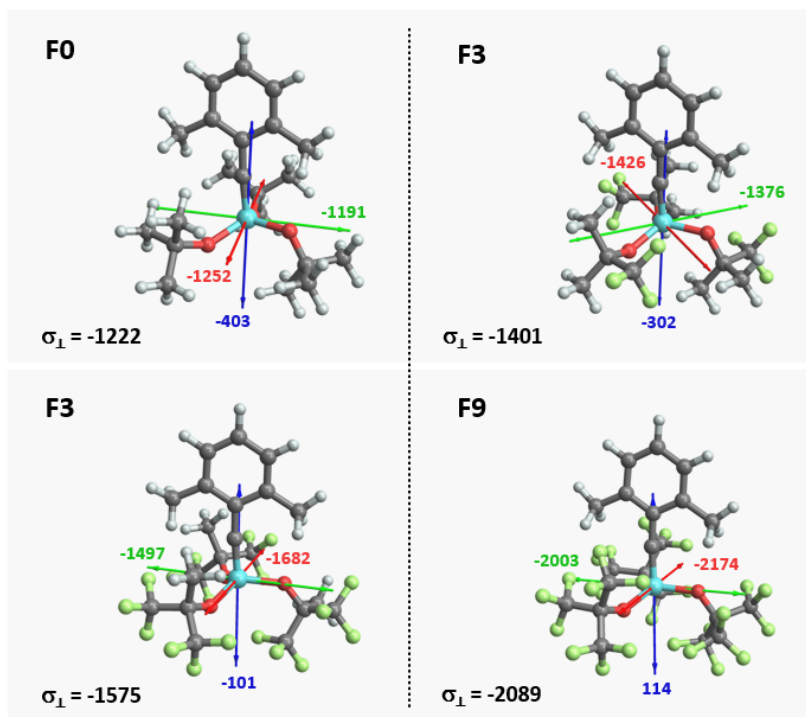


Figure S46. Shielding tensor orientations for the fluoroalkoxy-series. The depicted values represent the shielding along the three principal components of the respective shielding tensor. Color code:  $\sigma_{11}$  = red,  $\sigma_{22}$  = green and  $\sigma_{33}$  = blue.  $\sigma_{\perp}$  refers to the average of  $\sigma_{11}$  and  $\sigma_{22}$ .

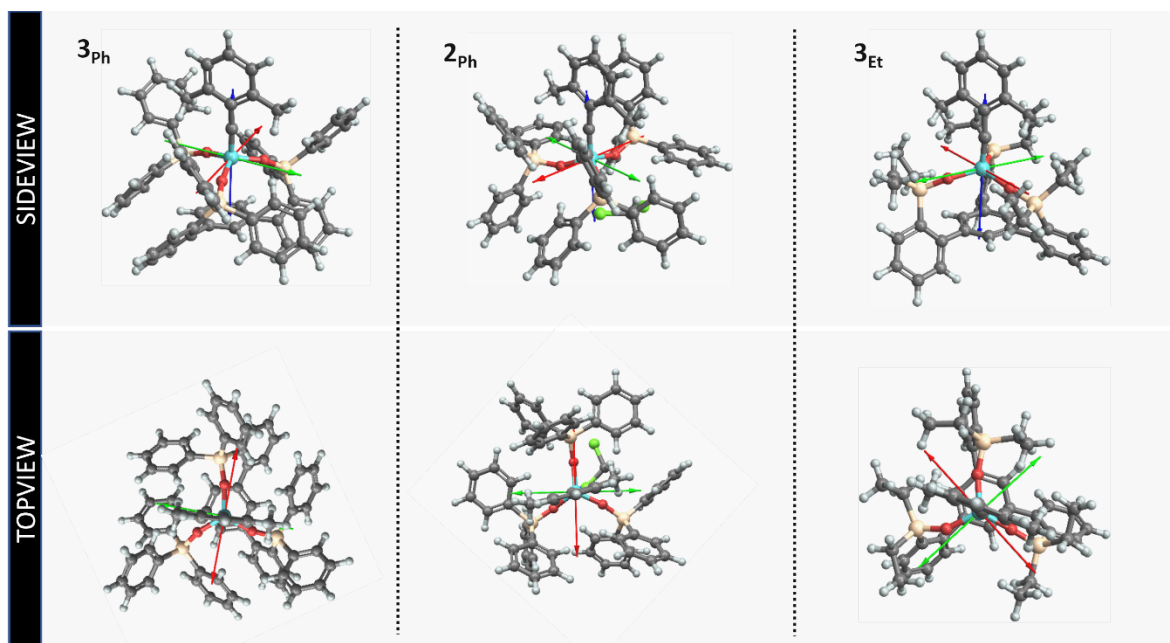


Figure S47. Shielding tensor orientations for silanolates  $\mathbf{3}_{\text{Ph}}$ ,  $\mathbf{2}_{\text{Ph}}$  and  $\mathbf{3}_{\text{Et}}$ . The colored arrows represent the shielding along the three principal components of the respective shielding tensor. Color code:  $\sigma_{11}$  = red,  $\sigma_{22}$  = green and  $\sigma_{33}$  = blue.

#### S4.4. Natural Chemical Shift analysis.

Nuclear shielding (and thereby chemical shift) tensors can be divided into diamagnetic and paramagnetic contributions, which also include contributions from spin-orbit coupling (Eqn. S1).<sup>22</sup> Diamagnetic contributions depend entirely on the occupied core orbitals (Eqn. S2) and are effectively independent of the ligands bound to the observed nuclei. They hence vary very little for the compounds studied here. In contrast, the paramagnetic contributions arise from pairs of occupied and vacant orbitals coupled through rotational operators (Eqn. S3). Deshielding of a tensor component along the direction  $i$  arises from coupling of an occupied orbital centered at the nucleus “superimposed” onto a vacant orbital by rotation of  $90^\circ$  (for p-type orbitals) or  $45^\circ$  (for d-type orbitals) along the axis  $i$ . Notably, the magnitude of deshielding increases with a decreasing energy gap between the two orbitals and paramagnetic shielding is therefore most strongly affected by frontier molecular orbitals (FMOs) – energetically high-lying occupied and low-lying vacant orbitals, as described by the Ramsey formalism:<sup>23</sup>

$$\boldsymbol{\sigma} = (\boldsymbol{\sigma}_{\text{dia}} + \boldsymbol{\sigma}_{\text{para+SO}}) \quad (\text{S1})$$

$$\sigma_{\text{dia},ij} = \frac{1}{2c^2} \sum_k \langle \Psi_0 | \sum_k (r_k^2 \delta_{ij} - r_{k,i} r_{k,j}) r_k^{-3} | \Psi_0 \rangle \quad (\text{S2})$$

$$\sigma_{\text{para},ij} = \frac{-1}{2c^2} \sum_n \sum_k \frac{1}{E_n - E_0} \langle \Psi_0 | \hat{L}_{k,i} | \Psi_n \rangle \langle \Psi_n | \hat{L}_{k,j} r_k^{-3} | \Psi_0 \rangle + c.c. \quad (\text{S3})$$

where  $\Psi_0$  and  $\Psi_n$  denote respectively the ground-state and  $n$ th excited state wave functions,  $r_k$  is the distance between the nucleus and electron  $k$ ,  $c$  is the speed of light,  $\delta_{ij}$  is the Kronecker delta function,  $\hat{L}_k$  is the angular momentum operator,  $E_0$  and  $E_n$  denote the energies of the energetic ground state and the  $n^{\text{th}}$  excited state, respectively and c.c. denotes the complex conjugate.

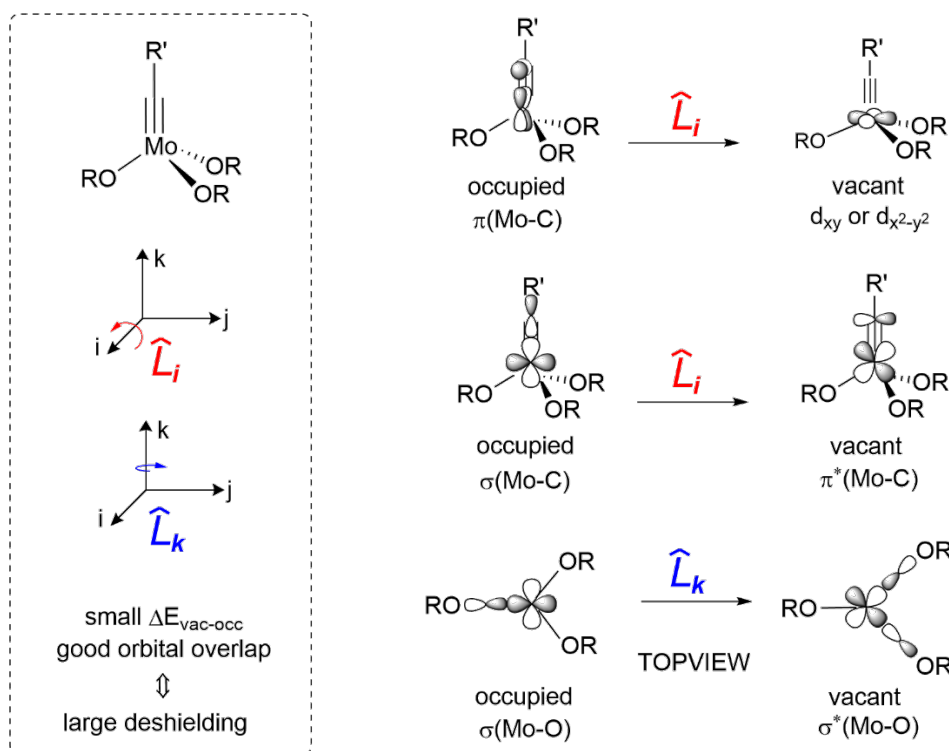


Figure S48. Schematic illustration of the rotational operators relevant to paramagnetic deshielding. An overview of the most important contributions to the three principal components  $\sigma_{11}$ ,  $\sigma_{22}$  and  $\sigma_{33}$  for a prototypical  $\text{Mo}(\text{CAr})(\text{OSiH}_3)_3$  ( $\text{Ar} = \text{Ph}$ ) can be found in Figure S48.

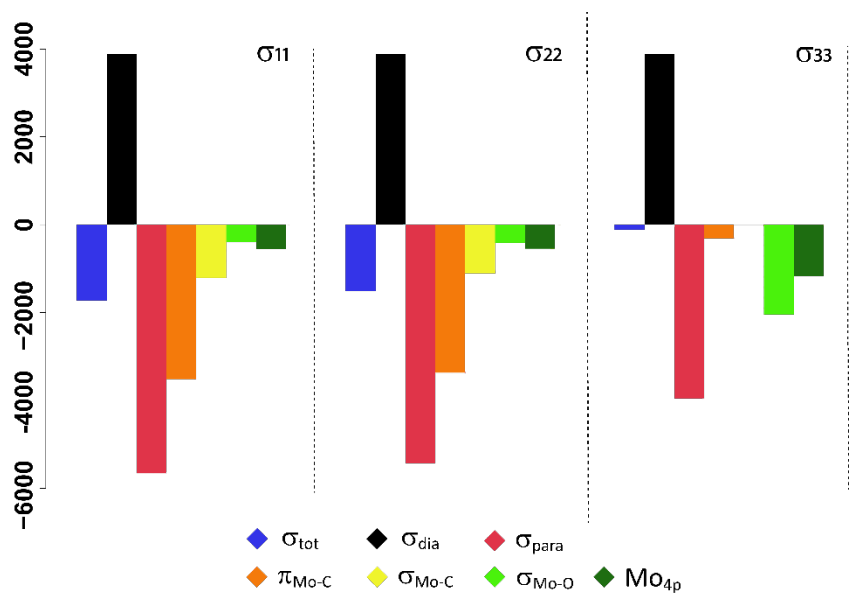


Figure S49. Natural chemical shift analysis of the principal components of  $\text{Mo}(\text{CAr})(\text{OSiH}_3)_3$  ( $\text{Ar} = \text{Ph}$ ).



Among the various orbital contributions, the coupling between the filled  $\pi(\text{Mo-C})$  and the empty  $\sigma^*(\text{Mo-O})$  is the dominant interaction, accounting for the strong deshielding of the  $\sigma_{11}$  and  $\sigma_{22}$  component. Relevant couplings for the  $\sigma_{33}$  component involve  $\text{Mo}(4p)$  and  $\sigma(\text{Mo-O})$  orbitals that are lower in energy and thus yield lower deshielding (see Figure S48).

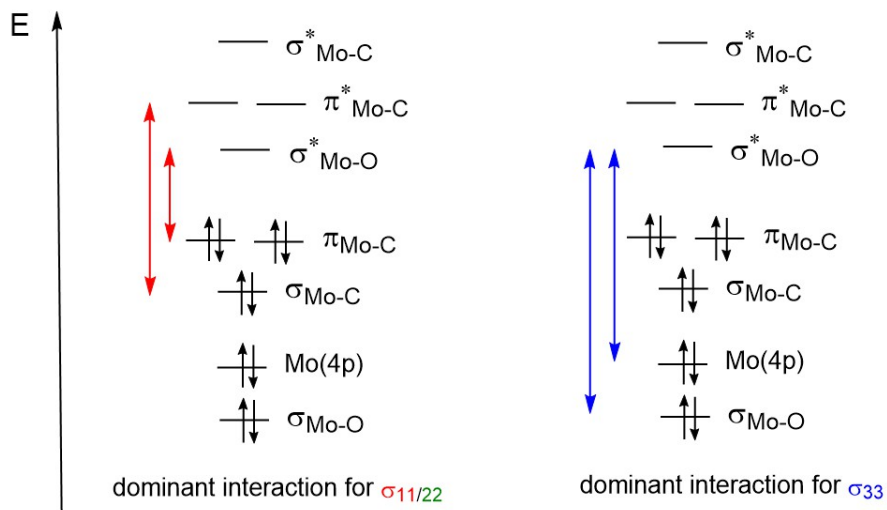


Figure S50. Simplified molecular orbital diagram highlighting relevant magnetic couplings.

We subsequently analyzed the influence of ligand electronegativity on the shielding tensor by NCS analysis. Therefore, we constructed small models of the type  $\text{Mo}(\text{CAr})(\text{OR})_3$  with  $\text{Ar} = \text{Ph}$  and  $\text{R} = \text{CF}_3, \text{SiH}_3$  and  $\text{CH}_3$  (see Figure S51 and S52).

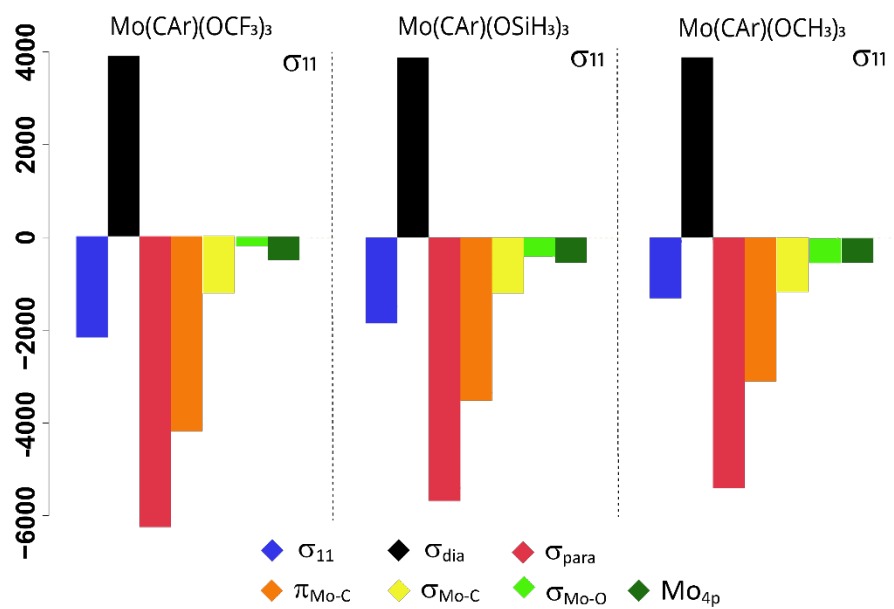


Figure S51. NCS analysis of the  $\sigma_{11}$  component of  $Mo(CAr)(OR)_3$  (Ar = Ph and R =  $CF_3$ ,  $SiH_3$ ,  $CH_3$ ).

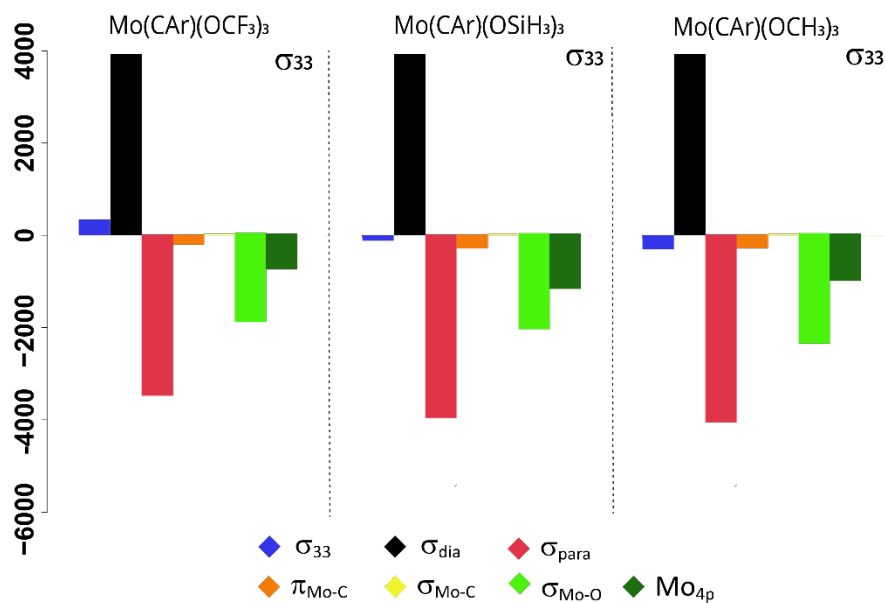


Figure S52. NCS analysis of the  $\sigma_{33}$  component of  $Mo(CAr)(OR)_3$  (Ar = Ph and R =  $CF_3$ ,  $SiH_3$ ,  $CH_3$ ).

Replacing the R group modulates the energy of the vacant Mo-O  $\sigma^*$  orbitals and hence the extent of deshielding. For  $\sigma_{11}$  and  $\sigma_{22}$  a more electron withdrawing ligand leads to more efficient deshielding, whereas for  $\sigma_{33}$  both empty and vacant orbitals are affected leading to a net shielding (see Figure S52).

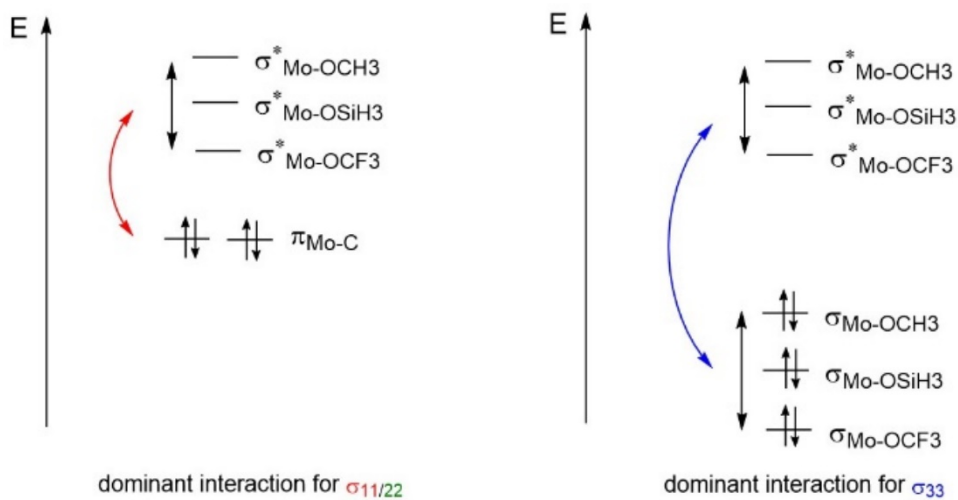


Figure S53. Simplified molecular orbital diagram highlighting the influence of ligand electronegativity.

S4.5. Calculated HOMO and LUMO energies of all complexes

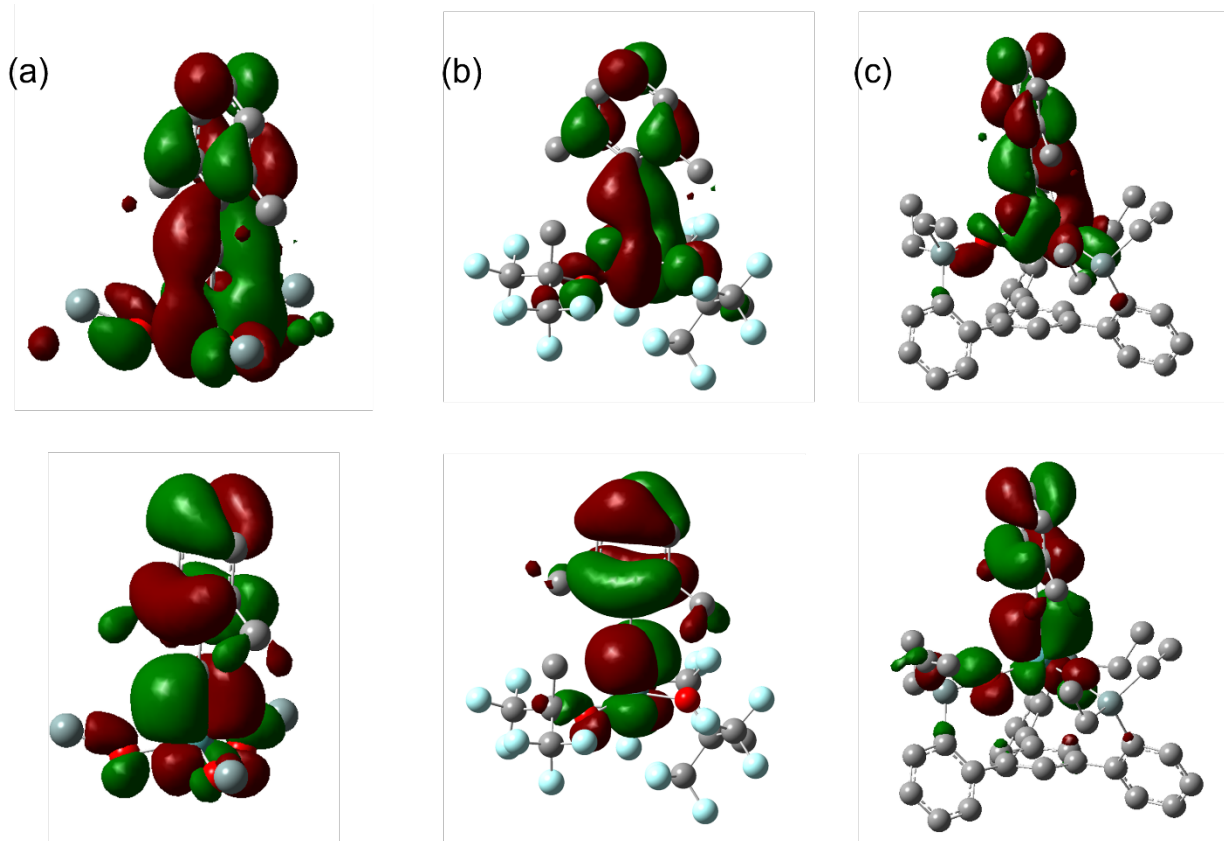


Figure S54. Calculated (bottom) HOMOs and (top) LUMOs of representative structures: (a)  $(\text{SiH}_3\text{O})_3\text{MoC}(\text{Ar})$ , (b)  $\mathbf{1}_{\text{F6}}$ , and (c)  $\mathbf{3}_{\text{Et}}$ . H atoms are not shown. The HOMOs and LUMOs of all compounds have similar structures, but are delocalized across the aromatic substituents of the silanolate ligand for  $\mathbf{3}_{\text{Et}}$ .

Table S4.2. Calculated HOMO and LUMO energies of all models (eV). Energies are normalized so that the HOMO of 1-phenyl-1-propyne is 0.000.

Model	HOMO	LUMO	HOMO-LUMO gap
(CH <sub>3</sub> O) <sub>3</sub> MoC(Ar)	0.243	4.599	4.356
(SiH <sub>3</sub> O) <sub>3</sub> MoC(Ar)	0.003	4.009	4.006
(CF <sub>3</sub> O) <sub>3</sub> MoC(Ar)	-0.8930	2.958	3.851
<b>1F0</b>	0.475	4.702	4.227
<b>1F3</b>	0.066	4.185	4.120
<b>1F6</b>	-0.463	3.639	4.101
<b>1F9</b>	-0.613	3.146	3.758
<b>2Ph</b>	0.459	4.250	3.791
<b>3Ph</b>	0.665	4.343	3.678
<b>3Et</b>	0.632	4.359	3.728
Diphenylacetylene	0.000	5.393	5.393

#### S4.6. Natural charge analysis.

Table S4.3. Natural charges on molybdenum for each alkylidyne resulting from natural population analysis

Model	Charge on Mo
<b>1F0</b>	1.31351
<b>1F3</b>	1.30788
<b>1F6</b>	1.30046
<b>1F9</b>	1.28198
<b>2Ph</b>	1.45726
<b>3Ph</b>	1.41811
<b>3Et</b>	1.44956

#### S4.7. Influence of geometry and ligand substituents on <sup>95</sup>Mo NMR parameters.

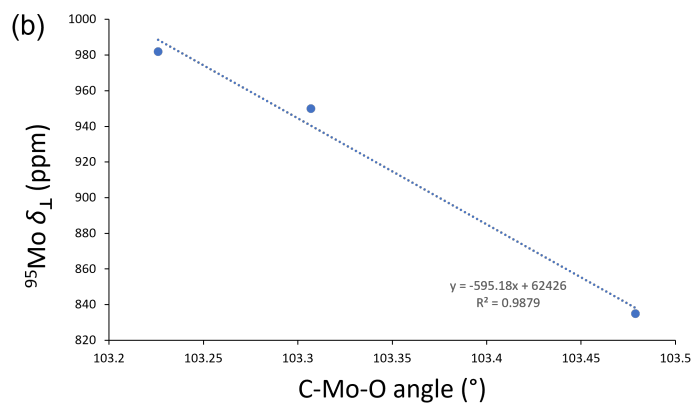
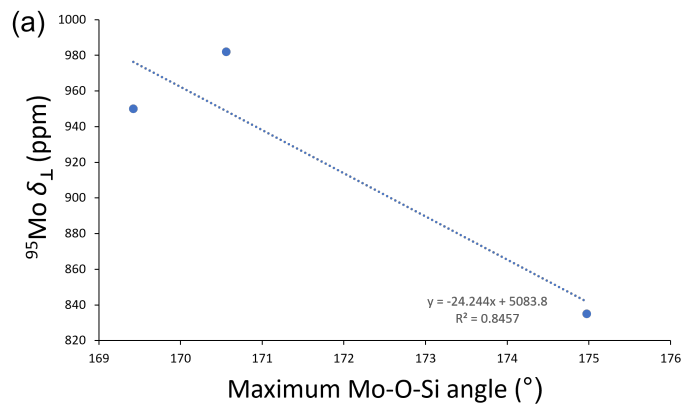


Figure S55. Correlation of  $^{95}\text{Mo } \delta_{\perp}$  to geometric parameters: (a) the largest (most linear) Mo-O-Si angle and (b) the corresponding C-Mo-O angle. Angles were extracted from the crystal structures of the silanolate compounds.

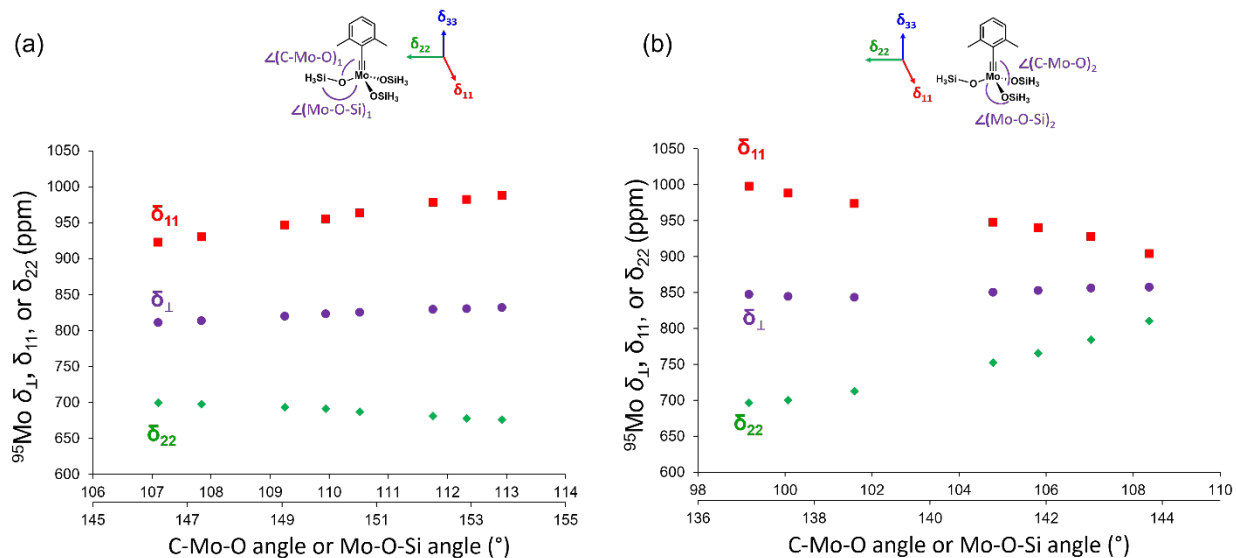


Figure S56. Calculated  $^{95}\text{Mo}$   $\delta_{11}$  (red),  $\delta_{22}$  (green), and  $\delta_{\perp}$  (purple) as a function of the varied Mo-O-Si angle or corresponding C-Mo-O angle for two different small computational model systems: (a) where the angles perpendicular to  $\delta_{11}$  were varied or (b) where the angle parallel to  $\delta_{11}$  was varied. When a single Mo-O-Si angle is increased (made more linear), there is a linear deshielding of  $\delta_{\perp}$  overall. Interestingly,  $\delta_{11}$  and  $\delta_{22}$  respond in opposite directions due to their dependence on orthogonal orbital couplings, though the net effect on  $\delta_{\perp}$  is deshielding. The magnitude of the changes in the  $^{95}\text{Mo}$  chemical shifts is approximately 5 ppm per degree change in Mo-O-Si bond angle.

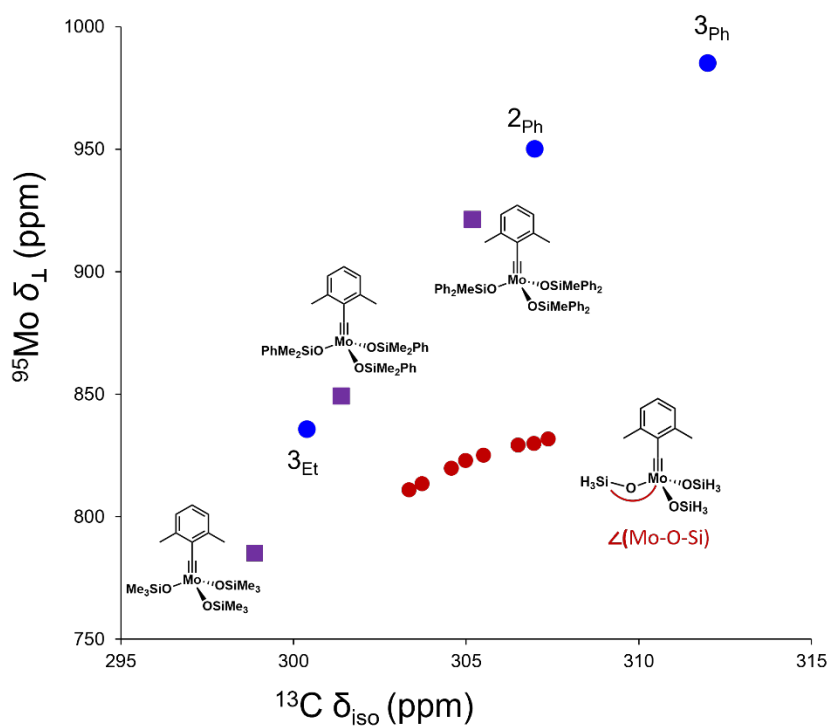


Figure S57. Plot of  $^{95}\text{Mo } \delta_{\perp}$  against the  $^{13}\text{C } \delta_{\text{iso}}$  of the alkylidyne carbon for the silanolate series (blue), computed siloxide model compounds with different Mo-O-Si bond angles (red, same models as Figure S54a), and small models having fixed geometries and different ligand substituents (purple).



## References

- (1) Harris, R. K.; Becker, E. D.; De Cabral Menezes, S. M.; Granger, P.; Hoffman, R. E.; Zilm, K. W. Further Conventions for NMR Shielding and Chemical Shifts (IUPAC Recommendations 2008). *Magn. Reson. Chem.* **2008**, *46* (6), 582–598.
- (2) Hillenbrand, J.; Leutzsch, M.; Yiannakas, E.; Gordon, C. P.; Wille, C.; Nöthling, N.; Copéret, C.; Fürstner, A. “Canopy Catalysts” for Alkyne Metathesis: Molybdenum Alkylidyne Complexes with a Tripodal Ligand Framework. *J. Am. Chem. Soc.* **2020**, *142* (25), 11279–11294.
- (3) Heppekausen, J.; Stade, R.; Kondoh, A.; Seidel, G.; Goddard, R.; Fürstner, A. Optimized Synthesis, Structural Investigations, Ligand Tuning and Synthetic Evaluation of Silyloxy-Based Alkyne Metathesis Catalysts. *Chem. - A Eur. J.* **2012**, *18* (33), 10281–10299.
- (4) Hillenbrand, J.; Korber, J. N.; Leutzsch, M.; Nöthling, N.; Fürstner, A. Canopy Catalysts for Alkyne Metathesis: Investigations into a Bimolecular Decomposition Pathway and the Stability of the Podand Cap. *Chem. - A Eur. J.* **2021**, *27* (56), 14025–14033.
- (5) Iuga, D.; Schäfer, H.; Verhagen, R.; Kentgens, A. P. M. Population and Coherence Transfer Induced by Double Frequency Sweeps in Half-Integer Quadrupolar Spin Systems. *J. Magn. Reson.* **2000**, *147* (2), 192–209.
- (6) Larsen, F. H.; Jakobsen, H. J.; Ellis, P. D.; Nielsen, N. C. QCPMG-MAS NMR of Half-Integer Quadrupolar Nuclei. *J. Magn. Reson.* **1998**, *131* (1), 144–147.
- (7) Schurko, R. W. Ultra-Wideline Solid-State NMR Spectroscopy. *Acc. Chem. Res.* **2013**, *46* (9), 1985–1995.
- (8) Massiot, D.; Fayon, F.; Capron, M.; King, I.; Le Calvé, S.; Alonso, B.; Durand, J. O.; Bujoli, B.; Gan, Z.; Hoatson, G. Modelling One- and Two-Dimensional Solid-State NMR Spectra. *Magn. Reson. Chem.* **2002**, *40* (1), 70–76.
- (9) Becke, A. D. Density-Functional Thermochemistry. III. The Role of Exact Exchange. *J. Chem. Phys.* **1993**, *98* (7), 5648–5652.
- (10) Hehre, W. J.; Ditchfield, K.; Pople, J. A. Self-Consistent Molecular Orbital Methods. XII. Further Extensions of Gaussian-Type Basis Sets for Use in Molecular Orbital Studies of Organic Molecules. *J. Chem. Phys.* **1972**, *56* (5), 2257–2261.
- (11) Roy, L. E.; Hay, P. J.; Martin, R. L.; Roy, L. E.; Hay, P. J.; Martin, R. L. Revised Basis Sets for the LANL Effective Core Potentials Revised Basis Sets for the LANL Effective Core Potentials. *J. Chem. Theory Comput.* **2008**, *4* (7), 1029–1031.
- (12) Gaussian 09; Revision D.01; Frisch, M. J.; Trucks, G. W.; Schlegel, H. B.; Scuseria, G. E.; Robb, M. A.; Cheeseman, J. R.; Scalmani, G.; Barone, V.; et al. Gaussian; Gaussian, Inc.: Wallingford CT, 2009.
- (13) Perdew, J. P.; Burke, K.; Ernzerhof, M. Generalized Gradient Approximation Made Simple. *Phys. Rev. Lett.* **1996**, *77* (18), 3865–3868.
- (14) Weigend, F.; Ahlrichs, R. Balanced Basis Sets of Split Valence, Triple Zeta Valence and Quadruple Zeta Valence Quality for H to Rn: Design and Assessment of Accuracy. *Phys. Chem. Chem. Phys.* **2005**, *7* (18), 3297–3305.
- (15) Grimme, S.; Antony, J.; Ehrlich, S.; Krieg, H. A Consistent and Accurate Ab Initio Parametrization of Density Functional Dispersion Correction (DFT-D) for the 94 Elements H-Pu. *J. Chem. Phys.*

- 2010**, 132 (15).
- (16) Marenich, A. V.; Cramer, C. J.; Truhlar, D. G. Universal Solvation Model Based on Solute Electron Density and on a Continuum Model of the Solvent Defined by the Bulk Dielectric Constant and Atomic Surface Tensions. *J. Phys. Chem. B* **2009**, 113 (18), 6378–6396.
  - (17) Velde, G.; Bickelhaupt, F. M.; van Gisbergen, S. J. A.; Guerra, C. F.; Baerends, E. J.; Snijders, J. G.; Ziegler, T. Chemistry with ADF. *J. Comput. Chem.* **2001**, 22 (9), 931.
  - (18) Barbieri, P. L.; Fantin, P. A.; Jorge, F. E. Gaussian Basis Sets of Triple and Quadruple Zeta Valence Quality for Correlated Wave Functions. *Mol. Phys.* **2006**, 104 (18), 2945–2954.
  - (19) Lenthe, E. van; Baerends, E. J.; Snijders, J. G. Relativistic Regular Two-component Hamiltonians. *J. Chem. Phys.* **1993**, 99 (6), 4597–4610.
  - (20) Glendening, E. D.; Landis, C. R.; Weinhold, F. NBO 6.0: Natural Bond Orbital Analysis Program. *J. Comput. Chem.* **2013**, 34 (16), 1429–1437.
  - (21) Hillenbrand, J.; Leutzsch, M.; Fürstner, A. Molybdenum Alkylidyne Complexes with Tripodal Silanolate Ligands: The Next Generation of Alkyne Metathesis Catalysts. *Angew. Chemie - Int. Ed.* **2019**, 58 (44), 15690–15696.
  - (22) Widdifield, C. M.; Schurko, R. W. Understanding Chemical Shielding Tensors Using Group Theory, MO Analysis, and Modern Density-Functional Theory. *Concepts Magn. Reson. Part A Bridg. Educ. Res.* **2009**, 34 (2), 91–123.
  - (23) Ramsey, N. F. Magnetic Shielding of Nuclei in Molecules. *Phys. Rev.* **1950**, 78 (6), 699–703.